

ISSN 0024-8266

mnassa

monthly notes of the astronomical society of southern africa

Volume 84 Nos 1-2

February 2025



In this issue:

News Notes: Dr Rosalind Skelton appointed Director of SAAO

Microlensing Conference

PRIME Telescope Opening

A Whisper of SN1987A

Re-imagining Wits Planetarium

Report on Solar Activity 2024

Observations of Comet 12P/Pons-Brooks

MNASSA free download site: www.mnassa.org.za

EDITORIAL BOARD	Mr Willie Koorts (Editor, <i>MNASSA</i>) Mr Auke Slotegraaf (Editor, <i>Sky Guide Southern Africa</i>) Mr John Gill (Webmaster) Dr Christian Hettlage (Web Manager) Dr I.S. Glass (Member, S A Astronomical Observatory) Mr Maciej Soltynski (Book Review Editor)
MNASSA PRODUCTION	Dr Ian Glass (Assistant Editor) Mr Willie Koorts (Publication on Web)
EDITORIAL ADDRESSES	MNASSA, PO Box 9, Observatory 7935, South Africa Email: mnassa@sao.ac.za MNASSA Download Page: www.mnassa.org.za
SUBSCRIPTIONS	<i>MNASSA</i> is available for free on the Internet
CONTRIBUTIONS	<i>MNASSA</i> mainly serves the Southern African astronomical community. Articles may be submitted by members of this community or by those with strong connections. Else they should deal with matters of direct interest to the community. <i>MNASSA</i> is published on the first day of every second month and articles are due one month before the publication date.
RECOGNITION	Articles from <i>MNASSA</i> appear in the NASA/ADS data system and are also available on Sabinet.

Cover picture: Comet C/2024 G3 (ATLAS) over Table Mountain on 19 January 2025
(W. Koorts)



mnassa

Vol 84 Nos 1-2

February 2025

News Note: Dr Rosalind Skelton appointed Managing Director of the SAAO

Dr Rosalind Skelton has been appointed the new Managing Director of the South African Astronomical Observatory (NRF-SAAO). She has held the position of Acting Managing Director of the facility since 2024, following the resignation of its previous MD, Professor Petri Vaisanen, who left to take up a position as the director of the Finnish Centre for Astronomy with ESO at Turku University.

Dr Skelton completed her Honours degree in Theoretical Physics at the University of Cape Town where she also completed her Master's degree through the National Astrophysics and Space Science Programme (NASSP). She then moved to the University of Heidelberg and the Max Planck Institute for Astronomy in Germany where she completed her PhD in Galaxy Formation and Evolution. After a stint as a postdoctoral Fellow at Yale University in the USA, she returned to South Africa in 2013 to take up a postdoctoral Fellowship at NRF-SAAO under the NRF's Professional Development Programme.

She joined the Southern African Large Telescope (SALT) Astronomy Operations team at NRF-SAAO in 2016 and was appointed as facility's Head of Research in 2023. Dr Skelton has been closely associated with NASSP for many years, as a supervisor, lecturer, as NRF-SAAO's NASSP representative, and as the Chair of the NASSP Partnership from 2021 – 2024.

She is an Honorary Research Associate of the University of Cape Town and has supervised a number of postgraduate students. Her group investigates the processes and interactions affecting galaxies in different environments through multiwavelength observations. Her work has led to more than 60 co-authored publications. She is also involved in a number of international research collaborations, including the 4MOST

Hemisphere Survey, where she is the science policy lead; as well as multiple large projects involving South Africa's flagship telescopes, SALT and the MeerKAT radio telescope.

In addition to her ongoing research and duties as the MD of NRF-SAAO, Dr Skelton co-chairs one of the science working groups of the LADUMA Large Survey Project on MeerKAT and is a member of the South African National Committee for Astronomy of the International Astronomical Union and South African Women in Science and Engineering. (NRF press release, 3 February 2025).



[Left to right] The Board Chairman of the National Research Foundation and Vice-Chancellor of the University of Cape Town, Prof. Mosa Moshabela, the newly appointed Managing Director of the (NRF-SAAO), Dr. Rosalind Skelton and the CEO of the (NRF) Dr Fulufhelo Nelwamondo at the official launch of the PRIME Telescope in Sutherland, Northern Cape on Friday 31 January 2025 (NRF photo).

News Note: International Microlensing Conference and Official Opening of PRIME Telescope

A conference on this topic was held 27-30 January 2025 at SAAO, followed by the official opening on 30 January of the PRIME Telescope at Sutherland. This is a collaboration involving the Dept of Science, Technology and Innovation of RSA, the NRF, SAAO, Osaka University, Astrobiology Center, (Japan), NASA Goddard Space Flight Centre, and the University of Maryland. The telescope has in fact been active for some time; the first observations of the Galactic Bulge having started in July 2023. Various delays to the project occurred because of the Covid epidemic and required lateral thinking to overcome them.

Gravitational Microlensing is a phenomenon whereby a massive object such as a planet or star bends and focuses the light from a more distant source behind it. When the lensing object passes in front of the more distant object its image may become brighter due to the addition of light from the background one. This is an effective technique for finding planets around distant stars that has the advantage over other methods of being sensitive to relatively small and low-mass objects. These are often too small to be detected by occultations or radial velocity changes. As a technique, because the phenomenon is so rare, it requires the precise photometric monitoring of huge numbers of stars in dense fields and searching for tell-tale variations in the light curves of each.

The most suitable field of densely packed stars is the inner Bulge of the Milky Way and most efforts to detect objects by microlensing have been concentrated there. The new PRIME telescope makes use of the infrared H band around 1.6 micrometres wavelength because light at this wavelength (about three times longer than visible) is less heavily obscured by the dense dust clouds near the centre of the Galaxy. Until relatively recently, infrared arrays had relatively small numbers of pixels, which limited the number of stars that could be observed simultaneously.

The PRIME telescope makes use of large area infrared detectors (type: HAWAII-4RG-10) developed for a future space satellite, the Roman Space Telescope, scheduled for launch in 2027. The future satellite will have an array of 18 detectors, giving 300.8 Megapixels. The sensitive layer of these detectors will be of HgCdTe. Four of these detectors, loaned by the Roman project, each of 4096 x 4096 pixels, are used in the PRIME camera that was provided by the University of Maryland and the Goddard Space Flight Center, partly funded also by University of Osaka. They are cooled to ~117K.

The telescope is a 1.8m diameter alt-azimuth built by Nishimura and commissioned by Osaka University. It has a primary mirror of F/2.29. To obtain a highly corrected field of 1.45 degree squared, it includes a 4-element lens correction system. It was partly funded by The Astro-Biology Center, Japan. The dome and building were funded by the University of Osaka and SAAO.

The data rate of the camera is 120 terabytes per year.

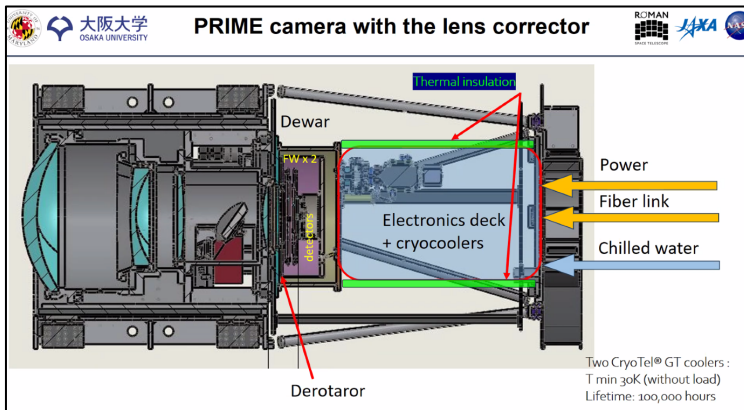


Fig 1: diagram of prime focus arrangement of telescope showing the 4-element corrector, image de-rotator, cooled camera and water-cooled top end containing the refrigerators and electronics.



Fig 2: Images of the PRIME telescope. The blue unit in the bottom left picture is the camera. Above it are the electronics and refrigeration units, themselves cooled to avoid air currents in the beam.

At last, a whisper of SN 1987A!

Magda Streicher

Earth is a mere speck in the Milky Way and to try and imagine and put it in perspective, is almost impossible. The soft band of the Milky Way is a reality that leaves one amazed with little understanding. Gazing southwards in favourable dark skies close to the

southern hemisphere summer we are able to see the two satellite Magellanic galaxies that revolve around our Milky Way/



Fig 1: Supernova 1987A, the titanic supernova explosion, first observed on 23 February 1987 just to the west of NGC 2070 as indicated in Johan Moolman's picture.

The star Sanduleak -69°202 was at magnitude 11.7 before the outburst. It blazed with the power of 100 million suns and brightened up to more than 2000 times what it was before. It was a blue supergiant, with a core collapse that should have left behind a neutron star, or a pulsar, but no evidence of that has yet turned up. Although the supernova itself is now a million times fainter, light echoes are beginning to show in the space surrounding it. Supernova 1987A was discovered independently by Ian Shelton and Oscar Duhalde at the Las Campanas Observatory in Chile on 24 February, 1987, and within the same 24 hours by Albert Jones in New Zealand, who has made over half a million variable star observations in his lifetime. He also discovered two comets. The Minor Planet (9171) was named in his honour, but he decided to name it Carlyndiane after his wife. What a wonderful gesture: to gift your wife with a piece of heaven!

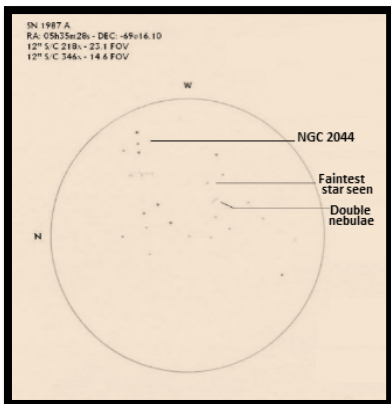
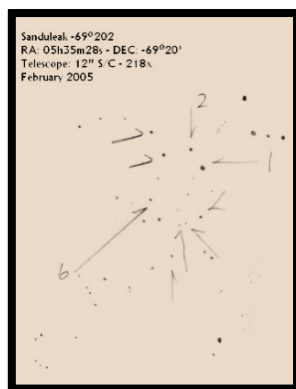


Fig 2: Author's first sketch of the area.



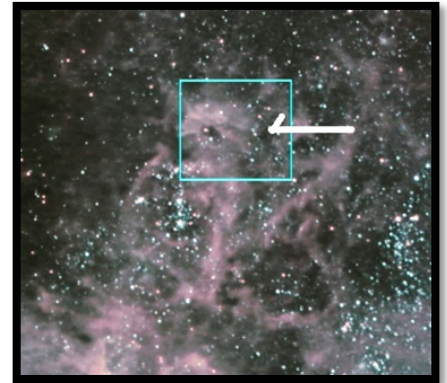
What are the chances of seeing a supernova outshine all the stars in the Milky Way? Probably not in my lifetime, I guess. The next best was one of the most outstanding sights I've ever seen, when a new star, now known as Supernova 1987A, appeared in the Large Magellanic Cloud. I fondly remember the Large Magellanic Cloud looking strange with the star embedded in the haze of our satellite galaxy, but the reality of a supernova in plain sight was an overwhelming experience. In 2005 I started searching the area in which this dying star once graced our skies.

Fig 3: Author's Second sketch (MS).

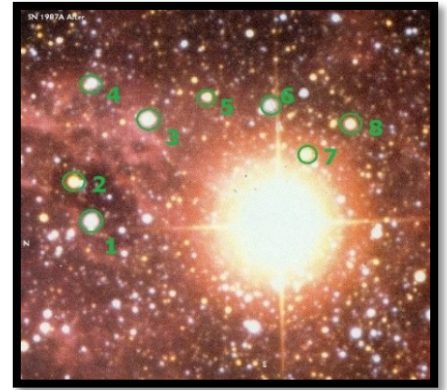
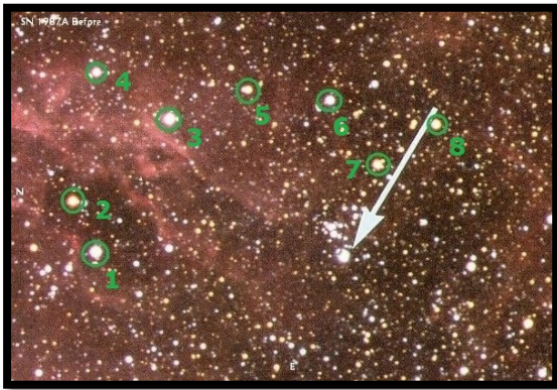
My very first sketch was very basic, randomly numbered to get familiar with the area.

(Right) Fig 3 (Johan Moolman)

The indicated double nebulosity in the next sketch (fig 3) was spotted in 2008 as shown in Johan Moolman's picture towards the top left inside the indicated box (fig 4, right). My magnitude limit was 12.5-13 with my 12-inch S/C telescope. The supernova's position is pointed out with an arrow in Johan's picture.



(Left below) Fig 5; (right below) Fig 6; (both D. Malin)



During 2012 my next approach was with my 16-inch S/C 350X telescope, with a visual magnitude limit of 14+ through my telescope during a night of excellent clear skies. I was able to identify, number and circle the stars around the supernova area (fig 4 and fig 5) in David Malin's book *View of the Universe* with the arrow showing the star Sanduleak -69°202 before and then after the outburst. Getting to know the area well was like old friends meeting again.

Identifications:

- Nr 1 Gaia EDR3 4657668522423399424 – magnitude 12.2
- Nr 2 Gaia EDR3 4657668492396164352 – magnitude 12.5
- Nr 3 Gaia EDR3 4657668866020783360 – magnitude 12.6
- Nr 4 Gaia EDR3 4657668870353280896 – magnitude 13.9
- Nr 5 Gaia EDR3 4657668732914348160 – magnitude 14.1
- Nr 6 Gaia EDR3 4657668694253739904 – magnitude 13.7
- Nr 7 Gaia EDR3 4657667942640388352 – magnitude 13.2
- Nr 8 Gaia EDR3 4657662818706888448 – magnitude 13.1

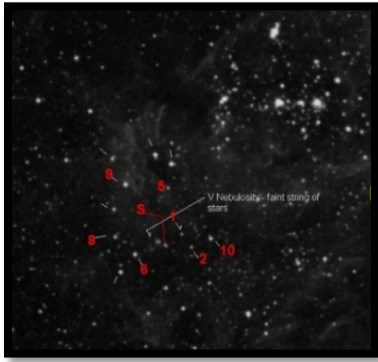


Fig 7: I contacted my friend Auke Slotegraaf, who sent me his numbered chart of the area (left). The open cluster NGC 2044 can be seen to the top right of the picture.

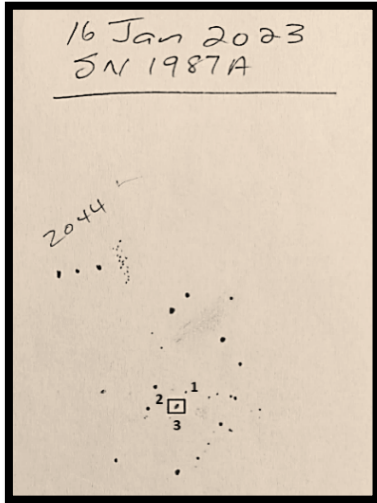


Fig 8: (sketch) I was excited but, not to get carried away with the find, I rather followed up year after year. I moved my 16-inch S/C towards the northern part of the Limpopo province with clear dark skies, with limiting magnitude through my 16-inch S/C telescope 15.6. With experience and dedication in January 2022, blessed with very dark skies, star-hopping, and with loads of patience, I achieved the nearly impossible: I could spot pieces of nebulosity between the stars and the faint fuzzy out of focus star at the exact location indicated as Gaia EDR3 4657668007030021248, and even the faint grouping Gaia EDR3 4657668075746867584 as a hazy faint star towards the north-west of the supernova. The extremely faint star Gaia EDR3 4657668080079343104, barely south of the supernova remnant was a faint something and only to be seen with averted vision. I used my rough sketches to show the progress in the indicated box and numbered it 1 to 3.

During May 2023, Tim Cooper and his wife Janet visited me on the farm, under excellent dark skies. With a friendship lasting more than 20 years we achieved and shared plenty of years of meteor counting and deep sky work. I was excited and could not wait to direct Tim towards this famous spot which he visually confirmed. What a joyful and overwhelming moment it was. Back home Tim overlaid the Hubble Space Telescope image onto Johan’s image (Fig 9). His comment: You can see SN1987A between the two stars – note the colour between them in Johan’s image. It started to

fade several years ago in x-rays, as the shock wave has now passed the limit of the ring and has moved into an area where the gas density is lower.

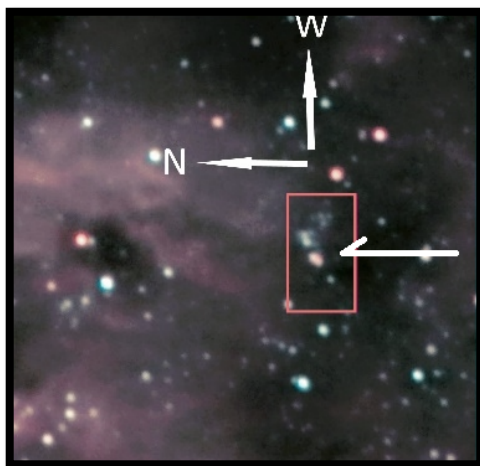


Fig 9. Credit: Johan Moolman.

Ref: “The Tale of Supernova 1987A”

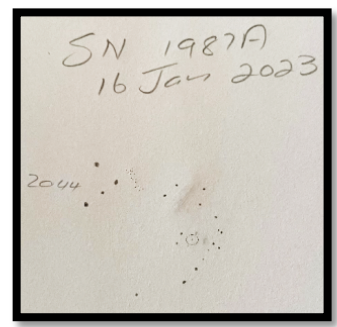
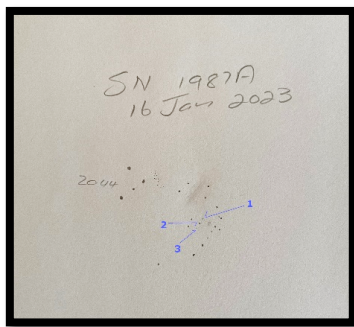
<https://chandra.harvard.edu/deadstar/sn1987a.html>

I wrote a letter to Brian Skiff, a well-known astronomer at Lowell Observatory in Arizona. His

dedication to amateurs is highly valued, and the help and advice he readily offers is endless.

“Greetings Brian, I hope you are doing just fine. Now, many years later, I have been able to identify the slightly elongated haze of Supernova 1987A between the faint field stars. I was excited and overwhelmed, and it was visually confirm by starry friend Tim Cooper. I moved my 16-inch S/C telescope to a very dark area in the western part of northern Limpopo with a super visual magnitude of up to 15+, and what a joy. I searched every little star with a lot of dedication around Supernova 1987A and found the out of focus hazy stars at the indicated location. I estimate two of them around magnitude 14+, with the middle one slightly more obvious, the other one a hazy out of focus impression. The fainter lower one as a faint something, only with averted vision as it barely came

in and out of view. Using from 290X to 462X, and a field of view from 10' to 17' with obvious nebulosity in the area.”



(left) Fig 10 ; (right) Fig 11

He replied:

“Greetings Magda; good to hear from you. I have had another look at the site of SN 1987A using modern catalogues. There is much new information now available! The two stars very close to the supernova are about mag 15. The one to the northwest is about V mag 15, while the one southeast is fainter, about V mag 15.7. I suspect you could see these only as a single star in your telescope, so the combined brightness is about 14.5. The small knot of stars to the northwest is possibly somewhat brighter, with combined brightness perhaps V mag 13 or so. I remember this was a complicated field for visual observing, so it is good that you were able to identify the target accurately”.

Nr 1 – The faint cluster to the north-west

Nr 2 – Yes, the middle ‘fuzzy star’ (your object 2) is the two stars flanking the supernova.

Nr 3 – This is a very faint star. You still have good eyes if you can see this star!”

Brian

At last, I could bathe in the joy of spotting the famous SN 1987A, even if it is only a whisper of the light echo seen through my trusty 16-inch telescope.

Magda

Re-imagining the Planetarium as the Wits Anglo American Digital Dome¹

William Martinson, Kate Otten Architects

Abstract: An architectural report on the modernisation of the Wits University Planetarium in Johannesburg.

The copper domed Wits Planetarium with its slender columned portico is a recognisable and well-known landmark on Yale Road on the East Campus of the University of the Witwatersrand. The Planetarium was completed in 1960 and was notable for its extraordinary Zeiss planetarium projector.

For over 60 years, the Planetarium, the largest in sub-Saharan Africa, has had a significant impact on the University and the broader community, with many thousands of visitors having experienced the projected celestial wonders. A high-profile Centenary project for Wits was to transform the Planetarium, into a fully interactive digital system. The newly named Wits Anglo American Digital Dome project aims to create a visualization laboratory within this iconic landmark. This will broaden its role well beyond astronomy, re-imagine its potential on a 21st Century campus, and enable unparalleled community engagement.

Kate Otten Architects (KOA) were appointed by the University of the Witwatersrand in 2021 as the architects for the adaptive re-use of the Planetarium. Noting the heritage importance and sensitivity of this building KOA appointed William Martinson as their specialist Heritage Architect.



Fig 1: Wits Planetarium – Wits Anglo-American Digital Dome (Kate Otten, Architects).

¹ *This article was produced from the architects' submission for the 2024 Herbert Prins Colosseum Awards and the text from the heritage application made to PHRAG of which William Martinson is the author.*



Fig 2: Location of Wits Planetarium – A landmark on Yale Road. (Kate Otten Architects).

History

The Festival Committee instituted to organise the celebrations in 1956 of the Seventieth anniversary of the founding of Johannesburg decided it

would be fitting to mark the occasion by raising the funds needed to buy and house a Zeiss Planetarium projector. It was however soon found that it would not be possible to obtain a new projector within a period of less than a year and it was decided to try and buy an existing one. With the assistance of Carl Zeiss in Germany, the Festival Committee succeeded in persuading the City Council of Hamburg to sell the projector which had been in use in that city since 1930, on condition that the projector would be fully modernised in the Zeiss factory.

The Hamburg projector was duly dismantled and moved to the Zeiss factory at Oberkochen for a complete overhaul. It was completely rebuilt with additional apparatus and improvements developed since its original construction - The result was a Zeiss Mk III Projector.

The responsibilities of the Festival Committee had in the meantime been taken over by the Johannesburg City Council who decided to sell the projector to the University of the Witwatersrand for use in the formal instruction of students and as a public amenity for the citizens of Johannesburg.

The architects R Spencer Parker, Anthony W. Parker and E N Finsen were duly appointed in 1958 for the Planetarium project. Evyind Niels Finsen was the project architect. Mr. C. A. Rigby was the consulting structural engineer. Once the architectural and structural documentation was complete, the contractor Desmond Davis was appointed, and building commenced in 1959.

A concrete dome approximately 22m in diameter, rests on a ring beam which is supported 5.5 m above floor level by the reinforced concrete wall on a structural concrete framework.

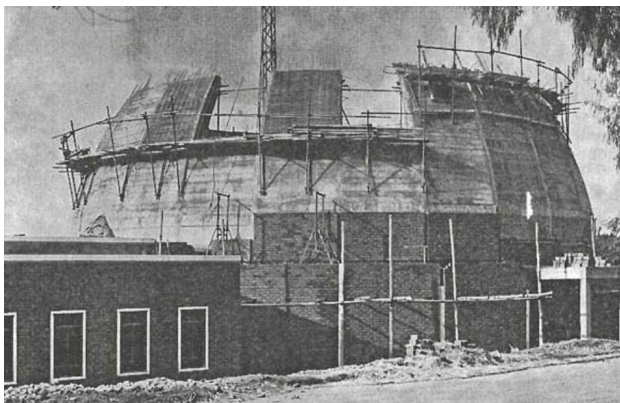


Fig 3: Planetarium under construction (Sourced by Kate Otten Architects).



Fig 4. Planetarium under construction (Sourced by Kate Otten Architects).

The dome was constructed in two stages, the first of which was ribbed and terminated in an intermediate ring beam and the second was the final hemispherical 'cap'. In order to simplify construction, the dome was divided into 24 equal segments.

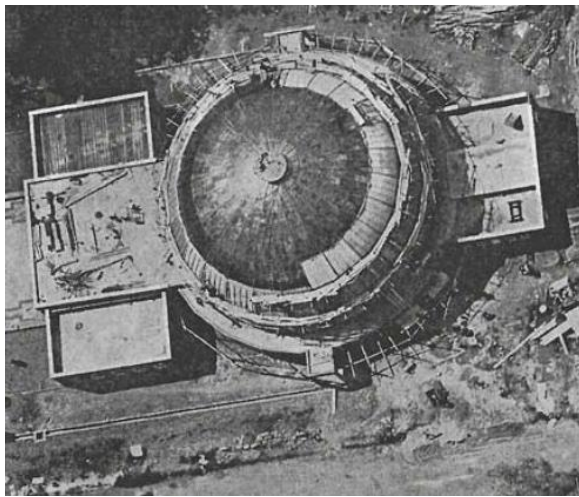


Fig 5. Planetarium under construction (Sourced by Kate Otten Architects).

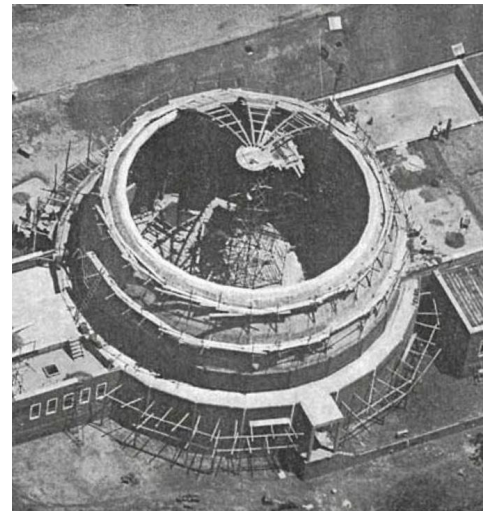


Fig 6. Planetarium under construction (Sourced by Kate Otten Architects).

The outer dome is covered with sheet copper - with welded seams - fixed to dovetailed wooden battens screeded into the concrete. The inner structure, the sheet aluminium projection screen, is fixed to a geodesic domed framework. There is sufficient space between the two domes for a person to stand upright.

The geodesic framework was made and erected for Carl Zeiss by Messrs Dyckerhoff and Wickman, who bought with them a mobile bridge scaffold, mounted on wheels which ran on a circular track on the floor of the auditorium. From appropriate platforms on this rotating scaffold, access to any portion of the geodesic dome was readily possible. The triangulated geodesic framework consists of several thousand flat steel bars interconnected by means of steel bolts. The lengths of the bars vary to give a perfect hemisphere on completion.

The erection of the complete geodesic framework and the fixing of the screen took two and a half months. To eliminate a 'whispering gallery' effect within the Planetarium, the aluminium sheets were perforated with approximately 30 million holes. In addition, a double layer of fibre glass wool insulation was wrapped round the outer surface of the framework. After the screen had been completed it was found that the disconcerting echoes, which were experienced from the outer concrete dome, had been entirely eliminated.

Entrance forecourt and loggia

The site of Planetarium is on the east side of Yale road - a few hundred metres to the north of the historic Yale Telescope building. Planning of the Planetarium was along an east-west axis with the dome placed centrally between the two rectangular annexes on the east and west sides. Externally the massing of the building comprises the large copper clad dome on a circular blue face-brick base bookended by two rectangular flat roofed pavilions.

Pedestrian entrance into the building from Yale Road was through a rectangular formal garden space defined by low perimeter walls, up a broad flight of steps through a symmetrical modernist hexastyle portico and then through a triple set of timber entrance doors into the large entrance foyer.

Each of the three timber doors was provided with a large clear glazed fanlight with decorative etched impressions of the Ophiuchus, Sagittarius and Perseus constellations.



Fig 7. Timber doors of planetarium with decorative etched impressions above (Kate Otten Architects).

The foyer was flanked on the north side by the Planetarium's administrative offices, a kitchenette, a small ticket office and a strong room. The male and female toilet facilities occupied the matching area on the south side. The seating in the planetarium was subdivided into six equal sectors with axial walkways between the banks of seating leading from each of the six double doors and terminating at a central oval island on which the projector stood. The dome was in turn flanked on the east side by a smaller scaled services wing.

Planetarium Projector

At the outset it was hoped that the planetarium would be ready for use during the Union of South Africa Jubilee Festival in May 1960. This was however not realized mainly due to the fact that the erection teams allocated by Messrs Carl Zeiss could not, due to commitments in other parts of the world, arrive in Johannesburg before the beginning of December 1959.

On completion of the building envelope the projector was installed and adjusted by a team of Zeiss technicians. On 12 October 1960 the first full-sized planetarium in Africa, and the second in the Southern Hemisphere, opened its doors to the public. The building has for the past 60 years served its function for a wide audience.



Fig 8. MkIII planetarium projector manufactured by Carl Zeiss of Germany (Sourced by Kate Otten Architects).

Adaptive re-use, alteration and additions

The brief was not only to transform the Planetarium into a cutting-edge digital facility, but also to provide for upgraded office spaces and teaching facilities. In addition, part of the brief was to add ablution facilities, a new access and upgrade the seating of the sports field and grandstands to the north of the Planetarium – the two facilities have long shared their position on campus. The different parts of the buildings were also to function as one or as separate, secure facilities in themselves. Some parts of the complex are also shared – like the viewing deck on the roof that is both a place to see the night sky through telescopes and an area for VIP guests to watch a match.

By all accounts a complex brief with an important heritage building to consider at the same time.

There are two main components to the project namely:

The adaptive re-use and restoration of the existing Planetarium building

The north wing extension.

Adaptive re-use and restoration of the existing planetarium building

To start, all sensitive and valuable heritage elements were protected or removed off site and re-installed later. This included the etched windows above the entrance doors, the entrance doors and handles, plaques, signage, ticket office window, marble skirtings, etc. A series of careful alterations to the internal spaces followed which included the removal of the current office spaces and kitchenette, to create a larger and grander foyer area. The existing ablutions were demolished internally and reconfigured for better functionality with and increased fixtures to meet current regulation requirements.

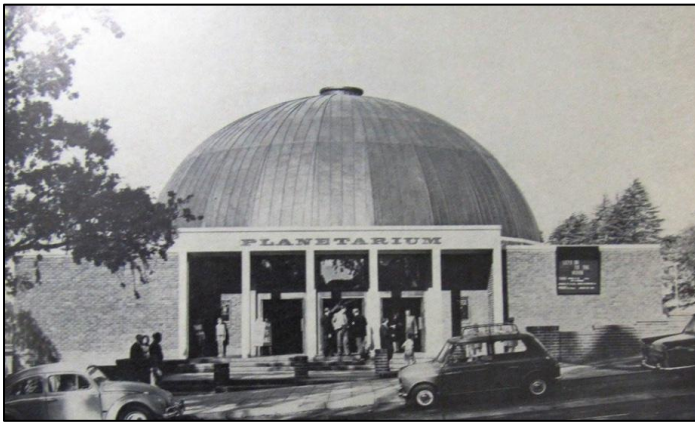


Fig 9. Old photograph of planetarium (Sourced by Kate Otten Architects).

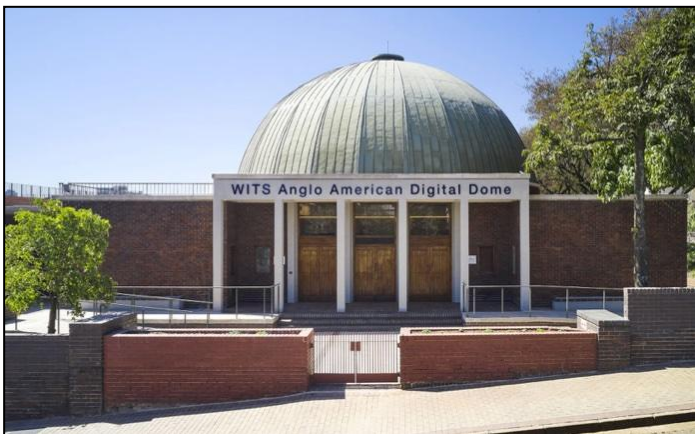


Fig 10. The main entrance now (Kate Otten Architects).

To the foyer we added a long seat, open plan kitchen area for events, and converted the original book store into a ticket office, using timber that we re-claimed and stored from the lab benches of the Gatehouse building – matching the Planetarium timber exactly.



Fig 11. The old Planetarium bookshop (Kate Otten Architects).

The circular passage around the dome or ambulatory was cleared of all dry walling and storage rooms, and restored to the original intended continuous space, with two additional fire

escape doors added to the northeast and southeast sections of the corridor to comply with current fire regulation.

The internal Planetarium domed aluminium projection screen has remained untouched with new projectors and equipment needed for the Digital Dome upgrade installed without affecting the existing screen or dome covering. The existing seating was removed and given to a school for re-purposing. This made way for a new raked seating arrangement required for the new Digital projections.

The historic Zeiss projector was carefully disassembled and packed and is currently being stored by the university with the intention of having the projector re-assembled in a new location on campus as a display/museum piece.

The original services and plant rooms located to the east of the building which were too small for the new equipment, have been extended to the east by an additional 3.5m in an unobtrusive manner with minimal impact on the main building.

The external facades and finishes of the existing building have been cleaned and repaired where necessary including colour matching the Marmoran finish – cracked and/or collapsing areas were rebuilt, repaired and coated in matching Marmoran.

The later addition of un-matching, stepped brickwork around the entrance courtyard was removed and the wall, entrance gate and planting re-done to include access ramps and seating. The additions maintain the symmetry about the central axis of the Planetarium and materials have been re-used or matched.

North wing extension

The addition to the north of the existing Planetarium building is a 3-storey building, care has been taken to ensure that all views of the dome from surrounding vantage points remain unobstructed, especially from Yale Road but also from the M2 highway.



Fig 12. Artist's impression of the North Extension of the Planetarium (Kate Otten Architects).

The setting out of both the height and plan lines of the new building, is taken from the original Planetarium building. The two structures are also separated a glazed entrance space, accessed by a ramp from the bottom of Yale road or from the original stairs from Yale road which have been extended in the same black brick.

The new and existing buildings, while working comfortably together, are legible as two distinct elements. The external facades of the new building are finished in terracotta-coloured patterned brickwork and the same Marmoran finish as the Planetarium, distinguishing it from the existing whilst referencing the masonry and other finishes of the existing building.



Fig 13. North Extension of the Planetarium (Kate Otten Architects).

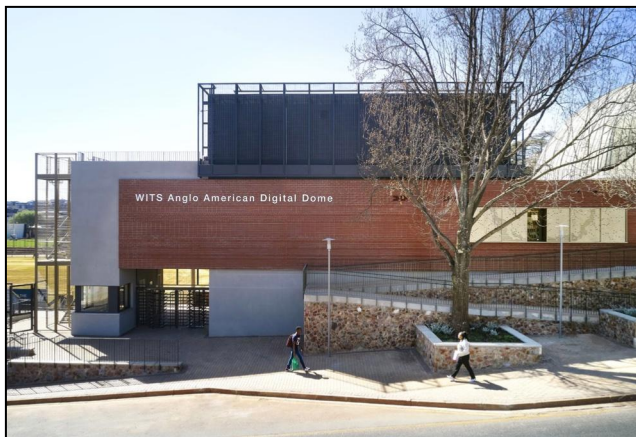


Fig 14. Old meets new at the Planetarium (Kate Otten Architects).

The lift and storerooms at roof level of the extension are covered in a steel mesh over which creepers are intended to grow thus referencing the bluey-green of the copper dome but not mimicking it. Another reference to the original building can be found in the sliding sun-screens which are patterned with the constellations of the night sky above the university, much like the etchings in the glass above the entrance doors.

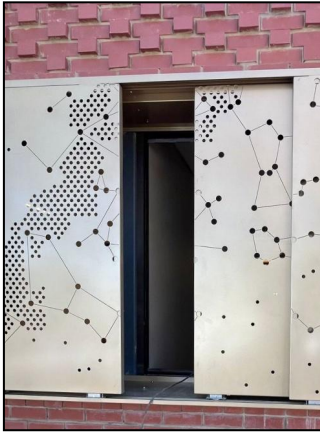


Fig 15. Star-patterned sliding sun-screens (Kate Otten Architects).

We believe that all people who visit the Digital Dome should be able to access the building equally and via the front door. We have therefore added ramps from the lower level of Yale road and other parts of Wits campus to ensure this is possible. The safety of children who are a large group of the visitors, has also been carefully considered.



Fig 16. Ramps at the Planetarium. Accessibility is a high priority (Kate Otten, Architects).

The Editors wish to thank Kate Otten and William Martinson for permission to reproduce this article, which previously appeared in The Heritage Portal Newsletter #37 2024.

<https://www.theheritageportal.co.za/article/re-imagining-planetarium-wits-anglo-american-digital-dome>

Unravelling the Sun: A Year of Solar Activity in 2024

Jacques van Delft. Director ASSA Solar Section

Abstract: This article explores the various solar activities observed throughout 2024 by the Astronomical Society of Southern Africa's (ASSA) Solar Section, focusing on sunspots, solar flares, coronal mass ejections (CMEs), and geomagnetic activities in Earth's atmosphere. The Solar Section of ASSA has carefully documented data on sunspot numbers, as well as C-, M-, and X-class solar flares, along with geomagnetic K and A indices.

The gathered data are analyzed and discussed in relation to existing scientific theories. ASSA's findings provide moderate evidence of correlations between sunspot numbers and solar flare activity, as well as between sunspot numbers and geomagnetic data. These relationships are examined in detail, offering valuable insights into the dynamic interactions between solar phenomena and their effects on Earth's space environment.

Glossary of Terms

Sunspots: Dark, cooler regions on the Sun's surface caused by intense magnetic fields that suppress heat transfer. Sunspots are indicators of the Sun's magnetic activity and often occur in cycles linked to solar phenomena like solar flares and coronal mass ejections.

Solar Flares: Sudden, intense bursts of electromagnetic radiation from the Sun, caused by the rapid release of magnetic energy in active regions near sunspots. Flares can affect Earth's atmosphere, causing radio blackouts and disruptions in communication systems.

Coronal Mass Ejections (CMEs): Large-scale eruptions of plasma and magnetic fields from the Sun's corona. CMEs are major drivers of geomagnetic storms on Earth and can disrupt satellites, power grids, and other technologies.

H-Alpha Observations: A method of observing the Sun using a specific wavelength of light (656.3 nm) emitted by hydrogen atoms. H-alpha imaging reveals detailed solar features, such as prominences, filaments, and flares, which are not visible in white light.

Solar Cycle: The approximately 11-year cycle of solar activity, marked by variations in the number of sunspots and solar phenomena. Solar cycles alternate between solar minimum (low activity) and solar maximum (high activity).

Maximum Daily Frequency (MDF): A statistical measure used in solar physics to represent the average daily number of sunspots over a specific period. It highlights trends in solar activity and helps in analysing solar cycles.

Solar Dynamo: The process within the Sun's convection zone that generates its magnetic field. It results from the interaction of plasma flows, rotation, and magnetic fields, driving solar phenomena like sunspots and flares.

Differential Rotation: A phenomenon where different parts of the Sun rotate at different speeds. For example, the equator rotates faster than the poles. This plays a key role in the Sun's magnetic field and solar dynamo.

Geomagnetic Storm: A temporary disturbance in Earth's magnetic field caused by solar wind or CMEs interacting with the magnetosphere. Effects include auroras, disruptions to satellites and power grid failures.

A and K Indices: A Index: A daily average of geomagnetic activity, indicating the overall disturbance in Earth's magnetic field. K Index: A 3-hour measure of geomagnetic activity on a scale from 0 (quiet) to 9 (extreme disturbance).

Space Weather

The environmental conditions in space, primarily influenced by the Sun, that affect Earth and its technologies. It includes phenomena like solar flares, CMEs, and geomagnetic storms.

Prominences and Filaments: Prominences: Large, bright loops of plasma extending outward from the Sun, held in place by magnetic fields. Filaments: Dark, thread-like structures visible against the solar disk, representing the same physical feature as prominences but viewed differently.

R² Value (Coefficient of Determination): A statistical measure that indicates how well data fits a regression model. For example: High R²: Strong correlation between variables. Low R²: Weak or no correlation.

Space Weather Prediction Centre (SWPC): A division of NOAA (National Oceanic and Atmospheric Administration) that monitors and forecasts space weather events, including solar activity and geomagnetic storms.

SILSO Program: The "Sunspot Index and Long-term Solar Observations" program, based in Belgium, collects and compiles global sunspot data, contributing to solar research and cycle predictions.

Solar Activity

Sunspots, the dark areas that occasionally manifest on the Sun's surface, were a central focus of solar observations in 2024. These cooler regions, caused by intense magnetic fields that suppress convective heat transfer, not only reflect the Sun's magnetic dynamics but also serve as critical indicators of overall solar activity. The Astronomical Society of Southern Africa (ASSA) highlighted the connection between sunspots and various solar phenomena, including solar flares and prominences. Sunspots appear darker because their temperatures are lower than the surrounding photosphere, a result of the magnetic fields obstructing heat flow from the Sun's interior. These

magnetic disturbances are also linked to significant solar events such as flares and prominences. (1)

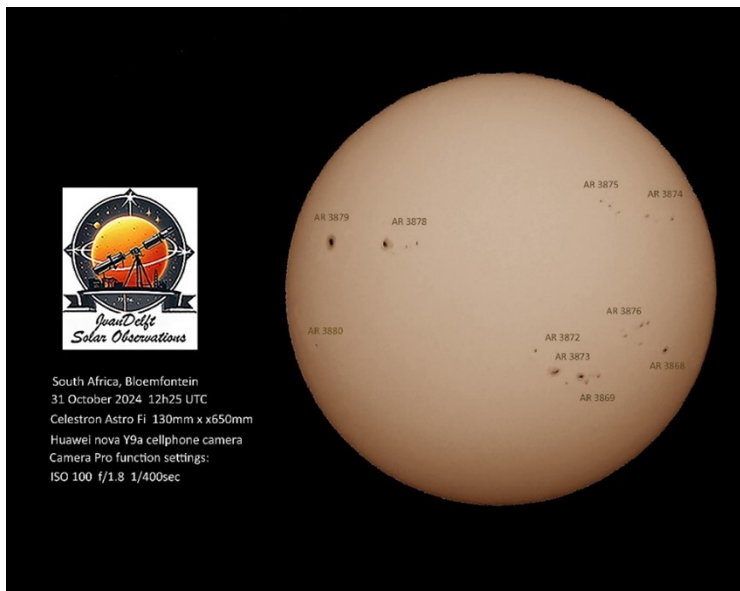


Fig 1. Sunspots 31 October 2024. Credit: JJ van Delft, ASSA.

Solar Flares: The Sun's Explosive Temper

Solar flares are sudden and intense bursts of radiation originating from the Sun's surface, resulting from the rapid release of magnetic energy. In 2024, detailed observations of these flares highlighted their strong

association with sunspot activity. These flares occur when twisted magnetic field lines in active regions near sunspots undergo a process of snapping and reconnection, releasing substantial amounts of energy. Several significant flares were recorded this year, offering valuable insights into the Sun's dynamic behaviour and its influence on space weather. Solar flares manifest as bright, abrupt emissions of light and energy across the electromagnetic spectrum, driven by the release of magnetic energy in regions of intense magnetic activity. (2)

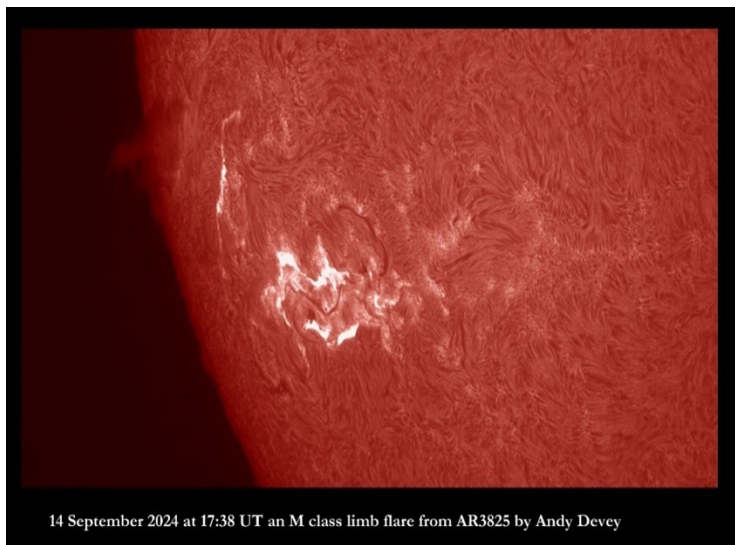


Fig 2. Flare 14 October 2024.: Credit: A. Devey, Spain, BAA – MSAS,

Coronal Mass Ejections: The Sun's Mighty Eruptions

Coronal Mass Ejections (CMEs) are massive eruptions of plasma and magnetic fields from the Sun, often observed as bright loops or expanding clouds in the solar

corona. These events are driven by the sudden release of magnetic energy in active regions, typically near sunspots or following solar flares. In 2024, some of the most striking solar phenomena recorded were CMEs.

CMEs are major drivers of geomagnetic activity, which can disrupt both space-based and terrestrial technologies and may also influence Earth's climate. When CMEs interact with Earth's magnetosphere, they can induce geomagnetic storms, potentially affecting satellite operations, communication systems, power grids, and navigation technologies. Additionally, some studies suggest that prolonged periods of increased geomagnetic activity may have subtle impacts on Earth's climate system. (3) Observations by the Astronomical Society of Southern Africa (ASSA) highlighted the frequent association between CMEs and preceding solar flare activity, underscoring the interconnected nature of these solar processes. (4)

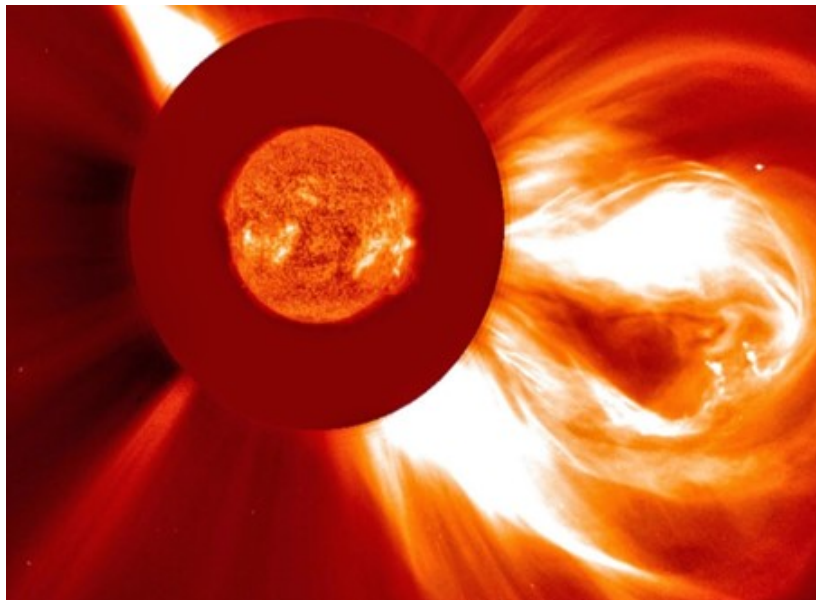


Fig 3. Coronal Mass Ejection.: Credit: NASA, ESA SOHO-LASCO

H-Alpha Observations: Peering into the Sun’s Secrets

Utilizing H-alpha telescopes, the ASSA team closely monitored several solar features, including prominences, filaments, sunspots, and plages. These observations provided a more

detailed picture of the Sun’s surface and its dynamic processes. The vivid imagery captured through H-alpha observations not only enriched the scientific community's understanding but also captivated the imagination of amateur astronomers.

In H-alpha images, prominences, filaments, and flares are vividly displayed. Prominences appear as bright loops or arcs of plasma extending outward from the Sun, while filaments are seen as dark, thread-like structures against the brighter solar disk.

Solar flares are visible as sudden bright flashes of increased light intensity. For example, an H-alpha image of the Sun can reveal the intricate structure of a solar prominence, showcasing the dense, cooler plasma suspended in the Sun's magnetic field. Such images are critical for understanding the complex magnetic interactions in the Sun's atmosphere that lead to various solar activities. (5)

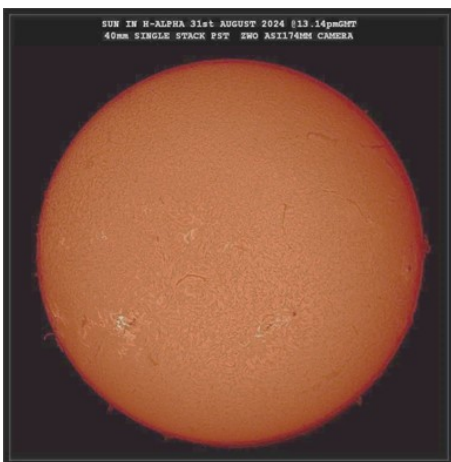


Fig 4. H α image 31 August 2024 Credit: Mick Nicholls, UK, BAA and MSAS

Analysis of Solar Cycles Progression

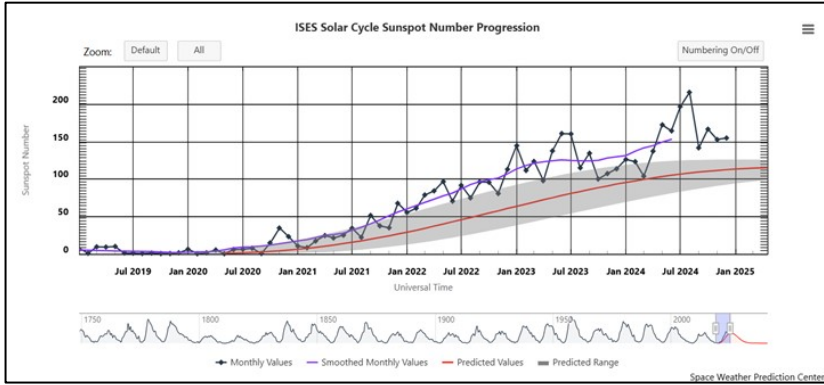


Fig 5. Current Sunspot cycle progression

<https://www.swpc.noaa.gov/products/solar-cycle-progression>

The graph in Fig 5 displays the progression of sunspot numbers over time, illustrating both observed monthly, smoothed values and predicted trends. Sunspot numbers are a key indicator of solar activity and are used to track the solar cycle, which typically spans approximately 11 years.

Solar cycle 25

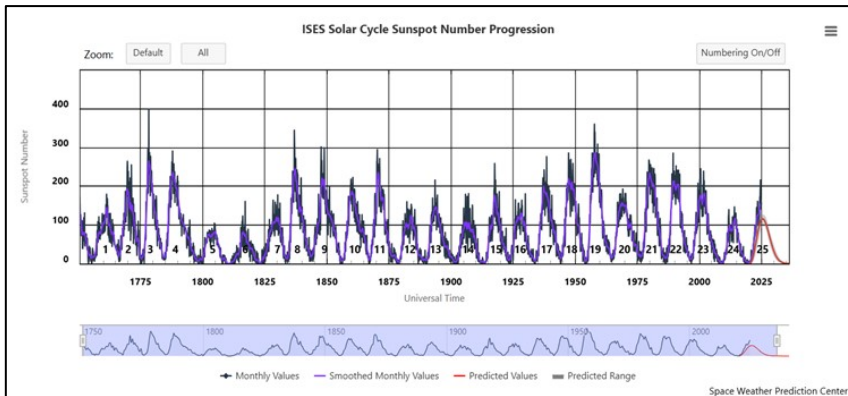


Fig 6. Multi-year sunspot numbers.

<https://www.swpc.noaa.gov/products/solar-cycle-progression>

From the graph in Fig 6, it's evident that sunspot numbers began to rise significantly after mid-2020, marking the onset of Solar Cycle 25. The smoothed monthly values (purple line) indicate a consistent increase in solar activity, reaching a peak around mid-2024. This peak is higher than the predicted values (red line), suggesting that Solar Cycle 25 might be more active than initially forecasted. The shaded area represents the predicted range, and the observed sunspot numbers have mostly remained within or slightly above this range, reflecting some variability in solar activity predictions. The rising trend is consistent with the natural progression of solar cycles, which involve alternating periods of solar maximum and minimum (6).

The Mean Daily Sunspot Number

The Mean Daily Sunspot Number, often referred to as the Mean Daily Frequency (MDF), is a statistical measure used to quantify the average number of sunspots observed on the Sun's surface over a specific period, usually a month. The MDF is a crucial tool in solar physics, providing a simplified representation of solar activity trends over time. In the context of the provided graph, the MDF can be derived from the monthly sunspot numbers and helps in understanding the overall activity level of the Sun during Solar Cycle 25. The graph's smoothed monthly values line (purple) essentially represents a form of the MDF, averaged to smooth out short-term fluctuations and highlight long-term trends in sunspot activity.

What is the Significance of MDF in Solar Cycle Analysis?

Trend Identification: MDF allows researchers to identify the phases of the solar cycle, including the solar minimum (low activity) and solar maximum (high activity), by providing a clear, averaged trend of sunspot numbers (7).

Solar Cycle Predictions: It helps in predicting the progression of the solar cycle. For instance, in the graph, the rising MDF values indicate increasing solar activity, signalling the approach and peak of the solar maximum (8).

Space Weather Forecasting: MDF is used to forecast space weather events, as higher sunspot numbers often correlate with increased solar phenomena like solar flares and Coronal Mass Ejections (CMEs), which can impact space and Earth-based technologies (9).

Understanding Solar Dynamo Processes:

The MDF reflects the efficiency of the solar dynamo, which generates the Sun's magnetic field. Comparing MDF values across cycles helps validate dynamo models and study solar asymmetries (e.g., activity differences between hemispheres) (10).

Climate Connections: Sunspot activity indirectly influences Earth's climate by modulating solar irradiance. The MDF serves as a proxy for variations in solar output over time (11).

Historical Solar Cycle Studies: The MDF is an essential parameter for reconstructing historical solar activity using archives and proxies like tree rings or ice cores, which reflect cosmic ray flux modulated by solar activity (12).

Why MDF is Important in the Graph:

The graph showcases both observed and predicted sunspot numbers, with the smoothed monthly values (similar to MDF) helping to illustrate the overall trend of Solar Cycle 25. This smoothing is essential for comparing actual observations with predictions, allowing scientists to assess the accuracy of solar cycle models and adjust forecasts accordingly.

For the smoothed monthly value in the graph the Mean Daily Sunspot Number (MDF) is used and calculated using the following formula:

$$\text{MDF} = \frac{\sum_{i=1}^n S_i}{n}$$

Where:

- S_i is the daily sunspot number for day i ,
- n is the total number of days in the period (usually a month),
- The summation \sum represents the total sum of the daily sunspot numbers over the period.

This calculation provides the average daily sunspot number, giving an overall measure of solar activity for the period in question. The MDF helps smooth out daily variations and highlights broader trends in solar activity (13).

How is data for the solar cycles obtained and by whom?

International Organisations: The sunspot data used by the Space Weather Prediction Centre (SWPC) comes from a combination of ground-based observatories, for example the NOAA's Solar Optical Observing Network and SILSO and space-based missions like the NASA's Solar Dynamics Observatory and SOHO. These sources provide consistent, high-quality data on sunspot numbers and solar activity (14).

Amateur solar observers: Amateur solar observers play a significant role in contributing to the sunspot data used by organizations like the Space Weather Prediction Centre (SWPC). Amateur astronomers equipped with safe solar observation tools (e.g., telescopes with solar filters) regularly observe and record sunspots. Many amateurs are part of coordinated networks such as the Royal Observatory of Belgium's SILSO program, which integrates their data into global sunspot records. Amateur observers help fill observational gaps caused by weather-related issues at professional observatories, geographic limitations (amateurs worldwide provide a more continuous coverage of the Sun) and their contributions ensure a higher frequency and consistency of daily observations.

Many amateurs have maintained personal sunspot records over decades, providing valuable data for studying historical trends and validating professional datasets. The SILSO program, which produces the international sunspot number, estimates that amateur observations contribute up to 50% of the daily sunspot reports in its network. Their observations are crucial for ensuring a global, consistent dataset that complements professional and satellite-based observations.

Amateur observers are an indispensable part of the sunspot monitoring effort, enhancing the resolution, reliability, and continuity of solar activity records (15).

The Importance of recording sunspots in both hemispheres.

Recording sunspots across both hemispheres of the Sun is fundamental in solar physics, as it provides critical insights into Understanding Solar Dynamo Mechanisms.

Sunspots are manifestations of the Sun's magnetic field and are directly linked to the solar dynamo process, which operates in the convection zone of the Sun. The solar dynamo is responsible for generating the Sun's magnetic field through complex interactions of plasma flows and magnetic fields

By documenting sunspots across both hemispheres, researchers are able to map the Sun's differential rotation, an essential component of dynamo theory (Howe, 2009). Additionally, analysing variations in sunspot numbers and magnetic activity between the northern and southern hemispheres offers valuable insights into asymmetries within the dynamo process (16).

It also helps with improving space weather predictions, gives Insights into Long-Term Solar and Terrestrial Interactions and helps protecting Modern Technology (17).

ASSA Solar Section Data Analysis: Year 2024

The Astronomical Society of Southern Africa (ASSA) Solar Section plays a pivotal role in monitoring and documenting solar activity. This dedicated section focuses on observing key solar phenomena, including sunspots, solar flares, and geomagnetic indices.

Each month, the section compiles and analyses solar images contributed by a small network of observers. These valuable observations and images are accurately curated to produce a comprehensive monthly Solar Bulletin, providing insights into the dynamic behaviour of our Sun and its influence on space weather. Reflecting on a year marked by heightened solar activity, it becomes crucial to analyse the collected data to uncover its scientific significance and assess the quality and standards of these observations.

Sunspot Data 2024

Year	Time	Seein	Grou	Spot	W no.	Nort	Sout	Nort	Sout
Wed	1205	G	10	42	142	2	8	13	29
Thu	1240	G	9	47	137	2	7	11	36
Fri	1245	G	12	41	161	3	9	8	33
Sat	1005	G	11	46	156	3	8	10	36
Sun					0				
Mon	1210	G	9	36	126	2	7	13	23
Tue	1300	G	7	18	88	2	5	10	8
Wed	1005	G	7	20	90	3	4	11	9
Thu	1110	G	11	34	144	6	5	23	11
Fri	1145	G	10	35	135	5	5	26	9
Sat	1100	G	6	16	76	4	2	13	3
Sun	1050	G	5	12	62	4	1	11	1
	Observations		Groups	Spots	W no.	North	South	North	South
	11		97	347	1317	36	61	149	198

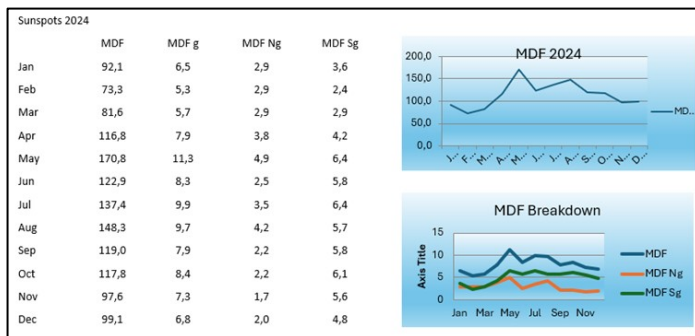
The ASSA solar section utilizes a standardized form to document solar observations systematically. The image (left) shows an example of the way data for sunspots are collected. For this study we are using the following components: Groups – Spots – W no. – North groups – South groups - North spots - South spots and the totals as on the bottom of the spreadsheet.(JJ van Delft ASSA solar section)

Monthly Means		
MDF	119,7	1 Observer
MDF g	8,8	1 Observer
MDF Ng	3,3	1 Observer
MDF Sg	5,5	1 Observer

From the data in the spreadsheet a monthly MDF is generated and recorded.

(JJ van Delft ASSA solar section)

Sunspot MDF data for 2024



(JJ van Delft ASSA solar section)

Key Observations

Overall Sunspot Activity (MDF)

The Mean Daily Frequency (MDF) shows significant monthly variation, with the highest activity in May (170.8) and the lowest in February (73.3).

Peak sunspot activity appears during the middle of the year, specifically from April to August, suggesting a possible phase of increased solar activity during these months.

Grouped MDF (MDF g)

Grouped MDF follows a similar trend as the overall MDF, peaking in May (11.3) and reaching its minimum in February (5.3).

The high value in May indicates a period of grouped sunspot occurrences, aligning with the peak in overall MDF.

Hemispheric Activity

Northern Hemisphere MDF (MDF Ng) shows relatively stable values throughout the year, fluctuating slightly between 1.7 (November) and 4.9 (May).

Southern Hemisphere MDF (MDF Sg) indicates more variability, with a peak in May (6.4) and a trough in February (2.4).

This suggests a more dynamic range of sunspot activity in the Southern Hemisphere compared to the Northern Hemisphere.

Seasonal Trends

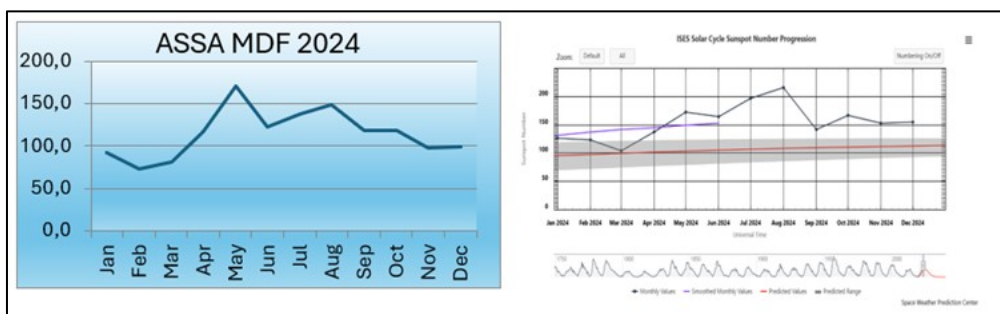
The data indicates a seasonal pattern, with heightened sunspot activity in the middle months (April to August), particularly noticeable in May.

Both hemispheres exhibit increased activity during this period, with the Southern Hemisphere showing slightly higher variability.

Conclusion

The 2024 sunspot data highlight a pronounced peak in solar activity during the mid-year months, especially in May. This period of increased activity is reflected across all measured metrics. The differences in activity between the Northern and Southern Hemispheres suggest potential hemispheric asymmetries in solar dynamics, which could be explored further for understanding the underlying solar processes.

Comparison between the ASSA MDF and official ISES solar cycle 25 progression.

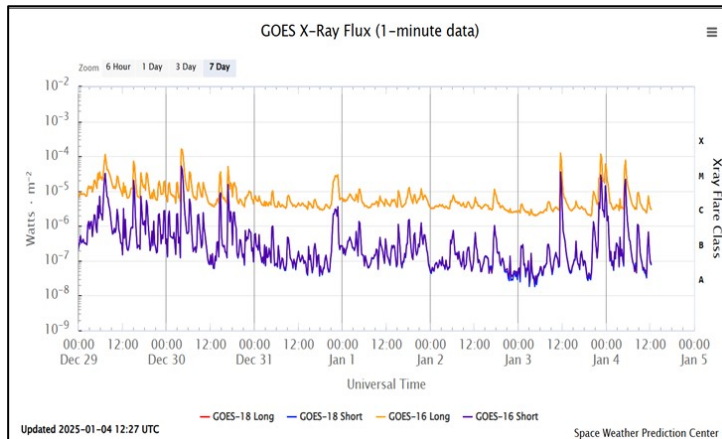


(JJ van Delft ASSA solar section)

While the ASSA "MDF 2024" focuses on Mean Daily Frequency, providing a more immediate and detailed look at sunspot frequency, the "ISES" graph provides a broader perspective, incorporating smoothed and predicted values. Despite these differences in detail and scope, the ASSA "MDF 2024" graph aligns well with the overall patterns

shown in the "ISES" graph, making it a good reflection of the same underlying solar activity trends.

Solar flare data 2024



<https://www.swpc.noaa.gov/products/goes-x-ray-flux>

Solar flares are classified based on their X-ray brightness in the wavelength range of 1 to 8 Ångströms. The classifications are:

A-Class: Weakest flares, producing the lowest levels of X-ray radiation.

B-Class: Slightly stronger but still minor flares with minimal impact on Earth.

C-Class: Moderate flares, they can cause small-scale disturbances in Earth's upper atmosphere.

M-Class: Medium-sized flares, can lead to brief radio blackouts and minor radiation storms.

X-Class: Strongest flares, capable of causing major radio blackouts, severe geomagnetic storms, and disruptions to satellites and power grids.

Each class has a scale from 1 to 9 (e.g., M1 to M9), and X-class flares can exceed this range, with numbers indicating intensity (e.g., X10). (SpaceWeather.com) (18).

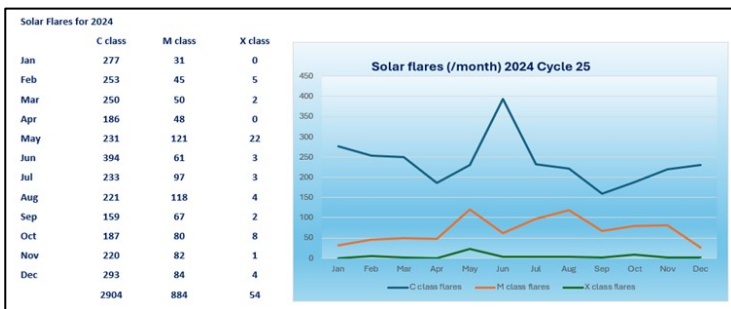
The ASSA solar section utilizes a standardized form to document daily the different solar flares systematically. The image below shows an example of the way data for daily solar flares are collected and recorded. For this study we are using the following components: Monthly totals for C class, M class and X class flares.

2024	November	C class	M class	X class	NOA No
Sun	22	11	3	0	3930/3932
Mon	23	5	2	0	3932/??
Tue	24	6	7	0	3930/3932/3938
Wed	25	6	3	0	3932/3938
Thu	26	4	1	0	3938
Fri	27	11	2	0	3928/3938
Sat	28	5	3	0	3932/3933
Totals		48	21	0	

M1,0/M1,0 M1,1
M8,9/M1,0
M1,0/M4,1 M1,1 M1,3 M1,0 M1,0/M1,2
M4,9/M2,8 M3,0
M7,3
M1,2/M3,3
M4,5 M1,3/M1,2

(JJ van Delft
ASSA solar
section)

Solar flare data 2024



This report presents an analysis of solar flare activity for the year 2024, categorized into C class, M class, and X class flares. The data covers the monthly distribution and total counts for each category, highlighting trends and peaks throughout the year.

(JJ van Delft ASSA solar section)

Key Observations

C Class Flares:

June experienced the highest number of C class flares (394). The lowest count occurred in September (159). Overall, C class flares were consistently high throughout the year.

M Class Flares:

May recorded the peak for M class flares (121), suggesting heightened moderate solar activity. The lowest number of M class flares was observed in April (48). Fluctuations were noticeable across different months.

X Class Flares:

May was the most active month for X class flares, with 22 occurrences. X class flares were relatively rare, with some months (January, April) recording none. A notable increase was observed in October (8).

Conclusion

The solar flare data for 2024 indicates significant variability in solar activity, with notable peaks in May and June. The increase in M and X class flares during these months suggests periods of intense solar activity that could influence space weather

and technological systems on Earth. This analysis is crucial for preparing and mitigating the potential impacts of solar flares.

Correlation Between MDF and Solar Flares

The correlation between sunspot MDF and solar flares arises because both phenomena are linked to the Sun's magnetic activity:

Active Regions: Active regions with high sunspot numbers and complexity often generate flares. The MDF, as a measure of sunspot activity, is therefore indirectly proportional to flare activity. Statistically, days with high MDF tend to coincide with increased flare activity, particularly C-class, M-class, and X-class flares.

Flare Productivity: Research shows that the number and intensity of solar flares scale with the size, complexity, and magnetic strength of active regions (e.g., Hale regions). Larger, more complex sunspot groups contribute to higher MDF values and are more likely to produce flares.

Temporal Trends: The relationship is evident on shorter timescales (days or weeks) and longer timescales (solar cycles). For example, during solar maxima, higher MDF values correspond to increased flare activity and intensity (19).

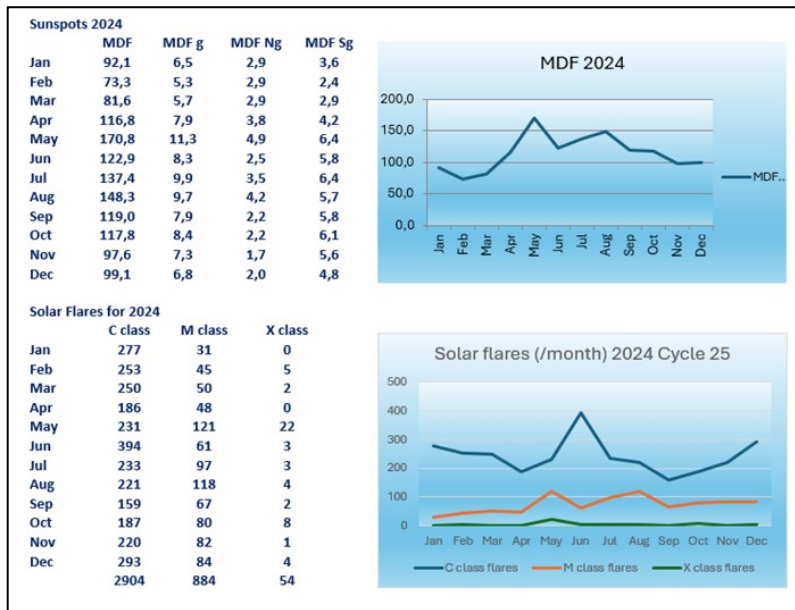
Quantitative Studies:

Flare Rates and MDF: Studies have found that regions with high sunspot numbers show a significantly increased rate of flaring activity. For instance, Tiwari et al. (2009) (20) demonstrated a positive correlation between sunspot complexity (which contributes to MDF) and the probability of major flares.

Solar Cycles and Activity: (Lisa M. Winter, Rick Pernak, K. S. Balasubramaniam (2016) (21) analyzed sunspot records and flares across multiple solar cycles, confirming that higher MDF values correspond with periods of increased solar flare frequency and intensity.

ASSA Data

Data for the different daily flare activity is obtained from the Laboratory of X-Ray Astronomy of the Sun.



(JJ van Delft ASSA solar section)

Analysis of MDF and C-Class Flares Correlation:



Left Chart: MDF - C Class Flares

Trend Observation: The chart shows the monthly variations of Maximum Daily Frequency (MDF) and the number of C-class flares for a specific year. Both the MDF and C-class flares exhibit fluctuations throughout the year. Peaks in C-class flares are visible around months 5 (May) and 6 (June), with another rise towards the end of the year. The MDF line also peaks during similar periods, although the correlation between the two is not consistently strong

Comparative Trends: There are some months where the trends of MDF and C-class flares appear to align (e.g., May and June), but in other months, such as the middle and end of the year, the trends diverge

Right Chart: Correlation MDF and C-Class Flares (Scatter Plot with Regression Line)

The scatter plot shows individual data points representing monthly MDF and corresponding C-class flare counts. A linear regression line is included, with the equation $y=0.099x+2.2161$ and $R^2=0$.

Correlation Analysis:

The slope of the regression line is positive, indicating a slight increase in C-class flares with higher MDF values. The R^2 value (0.012) is very low, suggesting a weak or negligible linear correlation between MDF and C-class flares. The data points are widely scattered, further supporting the lack of a strong linear relationship.

Notes:

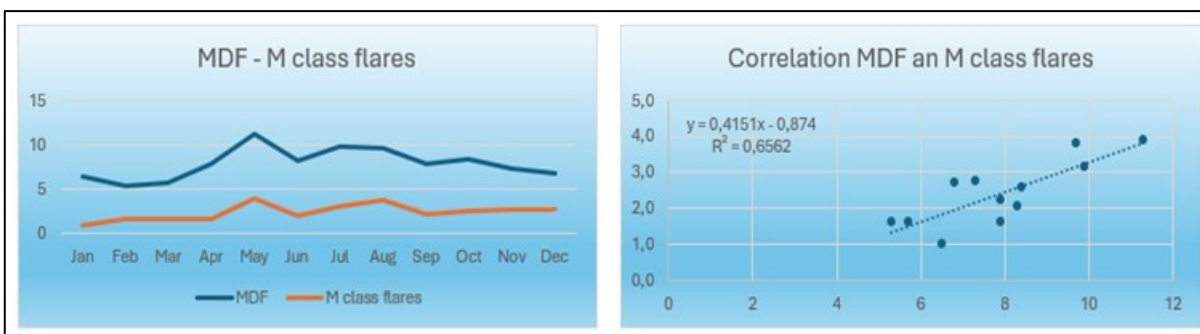
Weak Correlation: The analysis reveals a very weak correlation between MDF and C-class flares, as evidenced by the low R^2 value.

Inconsistent Trends: The monthly trends of MDF and C-class flares do not consistently align, leading to the weak correlation observed in the scatter plot.

Non-Linear Factors: Other factors likely influence C-class flare occurrences beyond what MDF alone can predict. This indicates a more complex relationship than what a simple linear regression can capture.

In summary, while there are some periods where MDF and C-class flares appear to align, the overall correlation is weak, suggesting that additional variables may be needed to fully understand the dynamics between sunspot activity and C-class flares.

Analysis of MDF and M-Class Flares Correlation



Caption: Credit JJ van Delft ASSA solar section

Left Chart: MDF - M Class Flares

Trend Observation:

This chart displays the monthly variations in the Maximum Daily Frequency (MDF) of sunspots and the number of M-class flares for a particular year. The MDF line remains relatively stable with small fluctuations throughout the year, showing peaks around

May and July. The M-class flares trend follows a similar pattern, peaking around May, although the fluctuations are more subtle compared to MDF.

Comparative Trends:

There is a general alignment between the peaks and troughs of MDF and M-class flares, suggesting a relationship between these two variables. The trends suggest that higher MDF values often correspond with increased M-class flare activity.

Right Chart: Correlation MDF and M-Class Flares

Scatter Plot with Regression Line:

The scatter plot presents individual monthly data points for MDF and M-class flares, with a fitted linear regression line. The regression equation is $y=0.4151x-0.874y$ and the R^2 value is 0.6562.

Correlation Analysis:

The positive slope (0.4151) indicates a positive relationship between MDF and M-class flares, meaning as MDF increases, M-class flare occurrences tend to increase. The R^2 value of 0.6562 suggests a moderate to strong linear correlation, indicating that around 66% of the variability in M-class flares can be explained by changes in MDF. The data points are more tightly clustered along the regression line compared to the C-class flares chart, indicating a clearer linear relationship.

Notes:

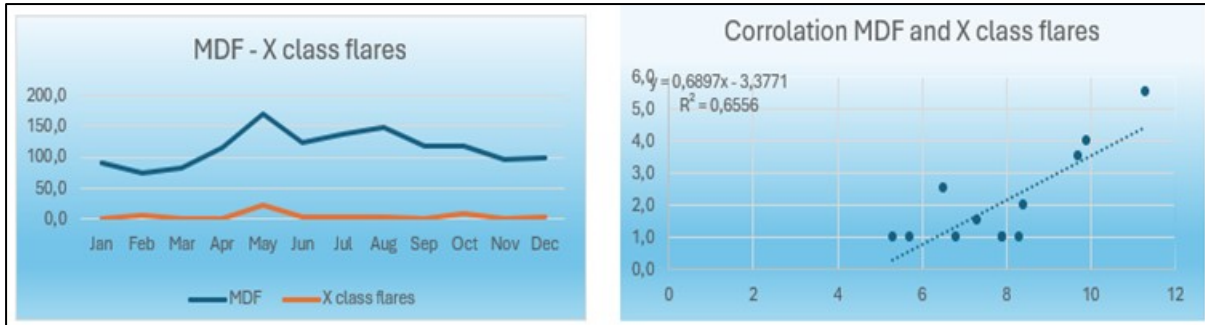
Moderate to Strong Correlation: The data shows a stronger correlation between MDF and M-class flares than with C-class flares. This suggests that MDF is a more reliable predictor for M-class flare activity.

Consistent Trends: The peaks in both MDF and M-class flares around the same months further support the observed correlation.

Linear Relationship: The moderate R^2 value and the positive slope indicate that the relationship between MDF and M-class flares can be reasonably captured with a linear model.

In summary, the analysis shows a notable correlation between MDF and M-class flares, with the linear regression model explaining a significant portion of the variability in flare activity. This suggests that higher MDF values are generally associated with increased M-class flare occurrences, reflecting a more predictable relationship compared to other flare classes.

Analysis of MDF and X-Class Flares Correlation



Credit JJ van Delft ASSA solar section

Left Chart: MDF - X Class Flares

Trend Observation:

The chart shows the monthly variations of the Maximum Daily Frequency (MDF) of sunspots and the number of X-class flares. The MDF trend has noticeable fluctuations, with peaks in May and July, indicating higher sunspot activity during these months. The X-class flares trend remains relatively low throughout the year, with minor increases, especially in May.

Comparative Trends:

While MDF shows significant peaks, the X-class flares trend is much flatter and does not exhibit sharp peaks, indicating that X-class flares are rarer and less frequent compared to sunspot activity. There is a slight alignment in May where both MDF and X-class flares peak, but the overall trend for X-class flares is much less pronounced.

Right Chart: Correlation MDF and X-Class Flares

Scatter Plot with Regression Line:

The scatter plot presents individual monthly data points for MDF and X-class flares, with a fitted linear regression line. The regression equation is $y = 0.6897x - 3.3771$, and the R² value is 0.6556.

Correlation Analysis:

The positive slope (0.6897) suggests a positive relationship between MDF and X-class flares, indicating that as MDF increases, the number of X-class flares also tends to increase. The R² value of 0.6556 indicates a moderate to strong linear correlation, meaning that around 66% of the variability in X-class flares can be explained by changes in MDF. The data points, while scattered, still show a trend along the regression line, indicating a notable but less tight linear relationship compared to M-class flares.

Notes:

Moderate Correlation: There is a moderate correlation between MDF and X-class flares, but due to the rarity of X-class flares, the correlation is less apparent in the direct comparison of trends.

Rarity of X-Class Flares: The low frequency of X-class flares compared to the more frequent sunspot activity (MDF) highlights the challenges in observing a strong correlation in small datasets.

Influence of Outliers: A few months with higher X-class flare occurrences (like May) significantly influence the correlation, which may not fully represent the overall trend. In summary, the analysis indicates a moderate correlation between MDF and X-class flares, with higher MDF values generally associated with increased X-class flare activity. However, due to the rarity of X-class flares, the correlation is less robust, and larger datasets or longer time frames may be needed to establish a clearer relationship.

Geo-Magnetic data (A index) 2024

Auroras, known as the Northern Lights (Aurora Borealis) in the Northern Hemisphere and the Southern Lights (Aurora Australis) in the Southern Hemisphere, are captivating natural phenomena occurring in polar regions. These light displays result from the interaction between the solar wind—streams of charged particles emitted by the Sun—and Earth's magnetic field (22).

Auroras provide critical insights into various scientific fields, including:

Solar-terrestrial interactions: They help in understanding how solar wind influences Earth's magnetic environment
Dynamics of Earth's magnetosphere: Auroras reveal information about the behaviour and structure of the magnetosphere, particularly during geomagnetic storms
Space weather impacts: The study of auroras contributes to understanding the effects of space weather on satellite systems, communication networks, and power grids (23).

Auroral activity is monitored using multiple techniques and indices that assess their intensity, location, and spread. Key methodologies include:

Visual observations: Ground-based eyewitness accounts and imagery. **Satellite data:** Space-based instruments capturing auroral emissions from above Earth. **Ground-based instruments:** Magnetometers and all-sky cameras provide detailed measurements of geomagnetic fluctuations and auroral intensity. **Geomagnetic indices:** Metrics like the Kp index and A index quantify geomagnetic activity based on variations in Earth's magnetic field caused by solar activity (24).

The Kp index measures global geomagnetic activity on a scale from 0 to 9, derived from the maximum fluctuations in the horizontal component of Earth's magnetic field at

mid-latitude observatories In contrast, the A index provides a daily average of geomagnetic activity, offering a broader view of geomagnetic conditions over time While both indices reflect Earth's magnetic response to solar activity, they serve different purposes in geomagnetic research and space weather monitoring (25).

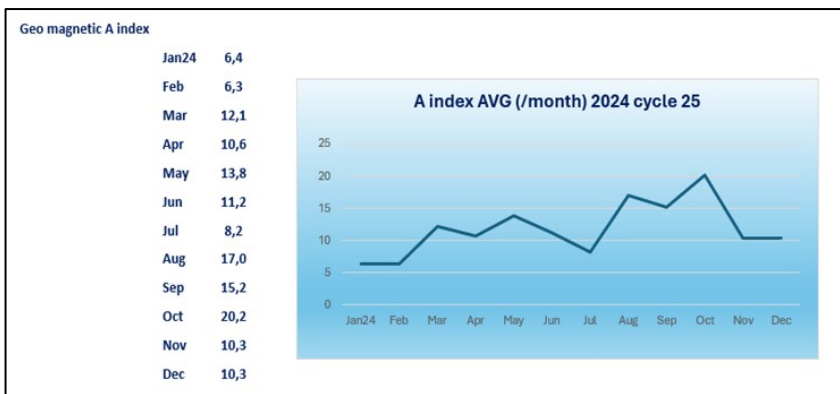
ASSA Geo-magnetic data 2024

The ASSA solar section utilizes a standardized form to document the K and A index systematically. The image below shows an example of the way data for K and A indexes

	0hrs to 03hrs	03hrs to 06hrs	06hrs to 09hrs	09hrs to 12hrs	12hrs to 15hrs	15hrs to 18hrs	18hrs to 21hrs	21hrs to 24hrs	A index
Nov 24									
23	2,00	1,67	1,67	1,67	3,00	1,67	2,33	1,67	8
24	1,67	1,67	1,67	1,00	0,67	1,67	1,67	3,67	7
25	3,33	2,33	2,00	2,33	2,67	3,00	2,33	2,33	11
26	3,33	2,33	1,00	1,33	1,00	0,67	1,00	2,00	7
27	1,00	0,67	1,67	2,00	0,67	1,00	1,00	2,33	5
28	2,00	1,00	0,67	1,00	0,67	0,67	1,00	0,33	4
29	1,67	2,33	1,67	2,33	2,00	1,33	2,67	2,67	8
30	4,67	3,33	2,33	0,67	1,00	0,67	1,00	2,33	11
Monthly Average									8

are collected and recorded. For this study we are using the following components: Monthly average of the A index. (JJ van Delft ASSA solar section)

ASSA data 2024



(JJ van Delft ASSA solar section)

The graph and accompanying data table highlight the monthly average A index

values for the year 2024. Here's a closer look at the key observations:

Low Activity at the Beginning of the Year: The year starts with relatively low geomagnetic activity, with the A index at 6.4 in January and 6.3 in February. These values suggest a calm geomagnetic environment, likely reflecting fewer disturbances from solar phenomena during this period.

Gradual Increase in Early Spring: In March, the A index jumps to 12.1, signalling an uptick in geomagnetic disturbances. This rise continues through April (10.6) and peaks in May at 13.8. This increase might be associated with higher solar activity, such as

more frequent solar flares or coronal mass ejections (CMEs), influencing Earth's magnetic field.

Summer Fluctuations: June sees a slight dip to 11.2, followed by a noticeable decrease in July at 8.2. However, August marks a significant spike to 17.0, indicating a period of heightened geomagnetic activity. This peak in August could be due to a series of solar events impacting Earth's magnetosphere.

Autumn Peaks: September continues the trend of high geomagnetic activity with an A index of 15.2, followed by the highest value of the year in October at 20.2. This period aligns with the increased likelihood of geomagnetic storms during the equinoxes, known for their potential to amplify solar wind effects on Earth's magnetic field.

Stabilization Towards Year-End: After the peak in October, the A index drops to 10.3 in both November and December, indicating a return to more moderate geomagnetic activity levels as the year concludes.

Analysis of MDF and A index Correlation



(JJ van Delft ASSA solar section)

Trend Analysis:

The A index, which reflects geomagnetic activity, shows variability with a notable peak in October. This suggests increased geomagnetic disturbances towards the latter part of the year.

Comparison with the MDF:

While there are similarities in the trend of both indices, the timing of their peaks does not perfectly align, indicating that geomagnetic activity may not directly correspond to solar flare activity.

Correlation MDF and A Index

Correlation Insights: The scatter plot displays a positive correlation between MDF and the A index, with the linear regression line showing a moderate upward trend.

Statistical Significance: The equation $y = 0.7095x + 3.696$ and an R^2 value of 0.2253 indicate a weak correlation. This suggests that while there is some relationship

between solar flare activity and geomagnetic disturbances, it is not strong enough to predict one based solely on the other.

Notes

Complex Interaction: The weak correlation highlights that geomagnetic activity is influenced by multiple factors, not just solar flares. This could include solar wind, coronal mass ejections (CMEs), and the Earth's magnetic field orientation.

Temporal Discrepancies: The difference in peak times for MDF and the A index suggests that geomagnetic responses may lag or depend on additional solar phenomena beyond flares alone.

The data reflects the dynamic and complex nature of space weather. While there is a visible relationship between solar activity (as indicated by MDF) and geomagnetic disturbances (A index), it is clear that multiple variables contribute to the overall picture. This reinforces the need for comprehensive monitoring and analysis to better understand and predict space weather impacts.

Conclusion

The quality of the ASSA Solar Section's data, which ranges from good to high, is an important factor in these findings. The consistency and precision of the recordings align well with internationally recognized standards of solar observation. This not only validates the methodology but also positions the ASSA Solar Section as a valuable contributor to the global effort in studying solar activity. It further demonstrates that relatively short observation periods can yield meaningful insights, especially when the data quality is high, and the analysis methods are rigorous.

Looking forward, as the ASSA Solar Section continues its monitoring efforts and extends its observational data over a more prolonged period, the potential for uncovering even stronger and more reliable correlations grows. This ongoing research will not only enhance our understanding of the Sun's complex behaviours but also improve our predictive models for space weather events. In turn, these models can help mitigate the effects of solar storms on modern technological systems, from satellite communications to power grids, ensuring that society remains prepared for the ever-present influence of solar activity.

In conclusion, while the short-term data from the ASSA Solar Section is a valuable starting point, it is the continued accumulation of high-quality observations that will provide the deeper insights needed to fully understand the Sun's behaviour. As the data grows, so too will our ability to predict and respond to solar phenomena, solidifying the importance of solar research in the context of both scientific discovery and practical application in our increasingly technology-dependent world.

References:

1. **Hathaway, D. H.** (2015). The Solar Cycle. *Living Reviews in Solar Physics*, 12(1), 4
- 4 **Schrijver, C. J., & Zwaan, C.** (2008). *Solar and Stellar Magnetic Activity*. Cambridge University Press.
2. **Shibata, K., & Magara, T.** (2011). Solar Flares: Magnetohydrodynamic Processes. *Living Reviews in Solar Physics*, 8(1), 6. **Benz, A. O.** (2017). Flare Observations. *Living Reviews in Solar Physics*, 14(1), 2.
3. **Pulkkinen, T.** (2007). Space Weather: Terrestrial Perspective. *Living Reviews in Solar Physics*, 4(1), 1. **Lockwood, M., Harrison, R. G., Woollings, T., & Solanki, S. K.** (2011). Are cold winters in Europe associated with low solar activity? *Environmental Research Letters*, 5(2), 024001.
4. **Gopalswamy, N.** (2016). History and development of coronal mass ejections as a key player in solar and geospace physics. *Geoscience Letters*, 3(1), 8. **Chen, P. F.** (2011). Coronal Mass Ejections: Models and Their Observational Basis. *Living Reviews in Solar Physics*, 8(1), 1. <https://doi.org/10.12942/lrsp-2011-1>
5. **Rutten, R. J.** (2003). Radiative Transfer in Stellar Atmospheres. *Lecture Notes on Stellar Atmospheres*, Utrecht University. Retrieved from https://robrutten.nl/rrweb/rjr-material/lecture_notes.php
- Fletcher, L., Dennis, B. R., Hudson, H. S., et al.** (2011). An Observational Overview of Solar Flares. *Space Science Reviews*, 159(1), 19-106.
6. **Hathaway, D. H.** (2015). The Solar Cycle. *Living Reviews in Solar Physics*, 12(1), **Pesnell, W. D.** (2012). Predictions of Solar Cycle 24. *Solar Physics*, 281(1), 507-532.
7. **Hathaway, D. H.** (2015). The Solar Cycle. *Living Reviews in Solar Physics*, 12(1), **Clette, F., & Lefèvre, L.** (2016). The New Sunspot Number: Assembling All Corrections. *Solar Physics*, 291(9-10), 2629-2651. Discusses the use of sunspot numbers for trend identification in solar cycle analysis.
8. **Pesnell, W. D.** (2012). Solar Cycle Predictions. *Living Reviews in Solar Physics*, 9(1). **Svalgaard, L., Cliver, E. W., & Kamide, Y.** (2005). Sunspot Cycle 24: Smallest Cycle in 100 Years? *Geophysical Research Letters*, 32(1).
9. **Tsurutani, B. T., & Gonzalez, W. D.** (1997). The Interplanetary Causes of Magnetic Storms: A Review. *Journal of Geophysical Research: Space Physics*, 102(A1), 141-164. **Schwenn, R.** (2006). Space Weather: The Solar Perspective. *Living Reviews in Solar Physics*, 3(1),
10. **Usoskin, I. G.** (2017). A History of Solar Activity over Millennia. *Living Reviews in Solar Physics*, 14(1); **Lean, J.** (2010). Cycles and Trends in Solar Irradiance and Climate. *Wiley Interdisciplinary Reviews: Climate Change*, 1(1), 111-122.

11. **Usoskin, I. G. (2017).** A History of Solar Activity over Millennia. *Living Reviews in Solar Physics*, 14(1); **Lean, J. (2010).** Cycles and Trends in Solar Irradiance and Climate. *Wiley Interdisciplinary Reviews: Climate Change*, 1(1), 111-122.
12. **Usoskin, I. G., Solanki, S. K., & Kovaltsov, G. A. (2007).** Grand Minima and Maxima of Solar Activity: New Observational Constraints. *Astronomy & Astrophysics*, 471(1), 301-309; **Beer, J., McCracken, K., & von Steiger, R. (2012).** Cosmogenic Radionuclides: Theory and Applications in the Terrestrial and Space Environments. *Springer*.
13. **Clette, F., & Lefèvre, L. (2016).** The New Sunspot Number: Assembling All Corrections. *Solar Physics*, 291(9-10), 2629-2651. **Hathaway, D. H. (2015).** The Solar Cycle. *Living Reviews in Solar Physics*, 12(1),
14. **Pesnell, W. D., Thompson, B. J., & Chamberlin, P. C. (2012).** The Solar Dynamics Observatory (SDO). *Solar Physics*, 275(1-2), 3-15. **Domingo, V., Fleck, B., & Poland, A. I. (1995).** The SOHO Mission: An Overview. *Solar Physics*, 162(1-2), 1-37. **Clette, F., Svalgaard, L., Vaquero, J. M., & Cliver, E. W. (2014).** Revisiting the Sunspot Number. A 400-Year Perspective on the Solar Cycle. *Space Science Reviews*, 186(1-4), 35-103.
15. **Clette, F., & Lefèvre, L. (2016).** The New Sunspot Number: Assembling All Corrections. *Solar Physics*, 291(9-10), 2629-2651. **Vaquero, J. M., & Vázquez, M. (2009).** The Sun Recorded Through History: Scientific Data Extracted from Historical Documents. *Springer*. **Hathaway, D. H. (2010).** The Solar Cycle. *Physics Today*, 63(12), 38-43. **Baranyi, T., Király, S., & Coffey, H. E. (2016).** Indirect Comparison of Debrecen and Greenwich Photoheliographic Results. *Monthly Notices of the Royal Astronomical Society*, 462(2), 1641-1647.
16. **Charbonneau, P. (2010).** Dynamo models of the solar cycle. *Living Reviews in Solar Physics*, 7(1), 3. **Howe, R. (2009).** Solar Interior Rotation and its Variation. *Living Reviews in Solar Physics*, 6(1), 1. **McIntosh, S. W., et al. (2013).** Hemispheric Asymmetries of Solar Activity: Nature's Grand Design. *The Astrophysical Journal*, 765(2), 146.
17. **Schrijver, C. J., et al. (2015).** Understanding space weather to shield society: A global road map for 2015–2025 commissioned by COSPAR and ILWS. *Advances in Space Research*, 55(12), 2745-2807. **Pesnell, W. D., et al. (2016).** The solar cycle and its impact on space weather. *Space Science Reviews*, 201(1-4), 3-44. **Eddy, J. A. (1976).** The Maunder Minimum. *Science*, 192(4245), 1189-1202.
18. **SpaceWeather**, <https://spaceweather.com/glossary/flareclasses.html>
19. **Leka, K. D., & Barnes, G. (2003).** Photospheric magnetic field properties of flaring versus non-flaring active regions. *The Astrophysical Journal*, 595(2), 1277. **Li, K. J., Feng, W., & Xu, J. C. (2018).** Statistical properties of solar flares and their relationships with sunspot numbers during solar cycles. *Research in Astronomy and Astrophysics*, 18(6), 63.

20. **Tiwari, S. K., Venkatakrishnan, P., & Gosain, S.** (2009). Sunspot groups and their flare productivity. *The Astrophysical Journal*, 702(1), L133.
21. **Lisa M. Winter, Rick Pernak, K. S. Balasubramaniam** (2016). Comparing SSN Index to X-ray Flare and Coronal Mass Ejection Rates from Solar Cycles 22–24
22. **Eather, R. H.** (1980). *Majestic Lights: The Aurora in Science, History, and the Arts*. **Milan, S. E., et al.** (2009). A superposed epoch analysis of auroral activity during magnetic storms. *Journal of Geophysical Research: Space Physics*.
23. **Kivelson, M. G., & Russell, C. T.** (1995). *Introduction to Space Physics*. Cambridge University Press. **Gonzalez, W. D., et al.** (1994). What is a geomagnetic storm? *Journal of Geophysical Research: Space Physics*. **Pulkkinen, A.** (2007). Space weather: Terrestrial perspective. *Living Reviews in Solar Physics*.
24. **Sandholt, P. E., et al.** (2002). The cusp and the cleft/LLBL: Local and global processes. *Space Science Reviews*. **Fiori, R. A. D., et al.** (2009). Empirical relationships between auroral electrojet indices and magnetometer data. *Space Weather*. **Bartels, J.** (1949). The standardized index, Ks, and its relationship to the geomagnetic indices K and Kp. *Journal of Geophysical Research*.
25. **Menvielle, M., & Berthelier, A.** (1991). The K-derived planetary indices: Description and availability. *Reviews of Geophysics*. **Rostoker, G.** (1972). Geomagnetic indices. *Reviews of Geophysics*.

Observations and images of Comet 12P/Pons-Brooks

Tim Cooper and Kos Coronaios

Summary

Comet 12P/Pons-Brooks became a fine object in the evening sky, emerging from the glare of the Sun during the second week of April 2024. Despite fading as it became higher each evening, the comet became visible to the naked eye during early May and was a fine object in binoculars. Images during late April and early May show a narrow ion tail around 3° in length and showing considerable changes in structure from night to night, as well as a broad fan-shaped dust tail. Dust was visible as an anti-tail 2° in length around the date Earth crossed the orbital plane of the comet on 6 June, following which the dust tail became the most prominent feature as the comet faded.

Introduction

Comet 12P/Pons-Brooks is a Halley-type comet, with a current period of 71.24 years (JPL). It was first discovered by Jean-Louis Pons on 21 July 1812, already bright at magnitude 4 (Chambó Bris 2024) and may have already undergone outbursts in activity prior to discovery. Encke determined the period of the comet as 70.68 years. The comet was re-discovered by William R Brooks on 2 September 1883 at magnitude 10 (Kronk 2008), but subsequently underwent three outbursts in brightness and peaked at magnitude 3 (Chandler 1883). During its third apparition in 1954, the comet experienced three outbursts in brightness, reaching a peak magnitude of 6 during April that year (Kronk 2024). All outbursts in brightness during the first three observed apparitions occurred prior to the comet passing perihelion. The 2024 apparition is the fourth recorded return of this comet, and the tendency to undergo outbursts in brightness pre-perihelion continued (James 2023, 2024), resulting in predictions the comet might become a naked eye object around perihelion on 21 April 2024. The comet was not visible from the southern hemisphere before perihelion but was expected to emerge from the solar glare around mid-April. Thereafter the comet would remain in the evening sky for several months, enabling observers from here to monitor its performance as it faded. This article provides a record of observations and images of comet 12P/Pons-Brooks received from southern Africa. Note all times are given in UT.

Details of the orbit

The 2024 apparition had the following osculating orbital elements (Epoch 2023-Sep-22.0 TDB, details from JPL Small Bodies Database):

Date of perihelion, T	2024 April 21.13132461
Perihelion distance, q	0.780864
Eccentricity, e	0.954561
Inclination of the orbit, i	74.190886
Longitude of ascending node, Ω	255.855252
Argument of perihelion, ω	198.987913

The comet has a highly inclined orbit, and with a Tisserand parameter of 0.60 is a typical Halley-type comet. Apart from perihelion on 21 April 2024 (distance from the Sun, $r = 0.78$ AU; distance from the Earth, $\Delta = 1.60$ AU), the comet made its closest approach to Earth on 2 June 2024 ($r = 1.10$, $\Delta = 1.546$), and Earth crossed the orbital plane of comet 12P four days later, on 6 June ($r = 1.15$, $\Delta = 1.548$). Closest approach to Earth occurred

at quite large distance compared to the minimum distance possible of $\Delta \sim 0.2$ AU for the pre-perihelion arc of the comet's orbit (Tomko and Neslušan 2016). Had closest approach to Earth occurred at this distance, and substituting Δ in the standard brightness equation $m_1 = 4.3 + 5 \log \Delta + 11.0 \log r$ (from Yoshida 2024) the magnitude of the comet might have been about 4.5 magnitudes brighter, reaching 1st magnitude.

First observations during April 2024

Comet 12P remained out of view for observers in southern Africa until early April. The nearby crescent Moon on 10 April aided in locating it, and on 13 and 14 April the comet was located just 3° to the left of Jupiter. First detection was by Lafras Smit in an image taken on 9 April, barely discernible in bright twilight and with the comet's altitude below 5° at the time. The following evening Lafras secured a second image, with the comet slightly more prominent despite strong twilight (Figure 1).

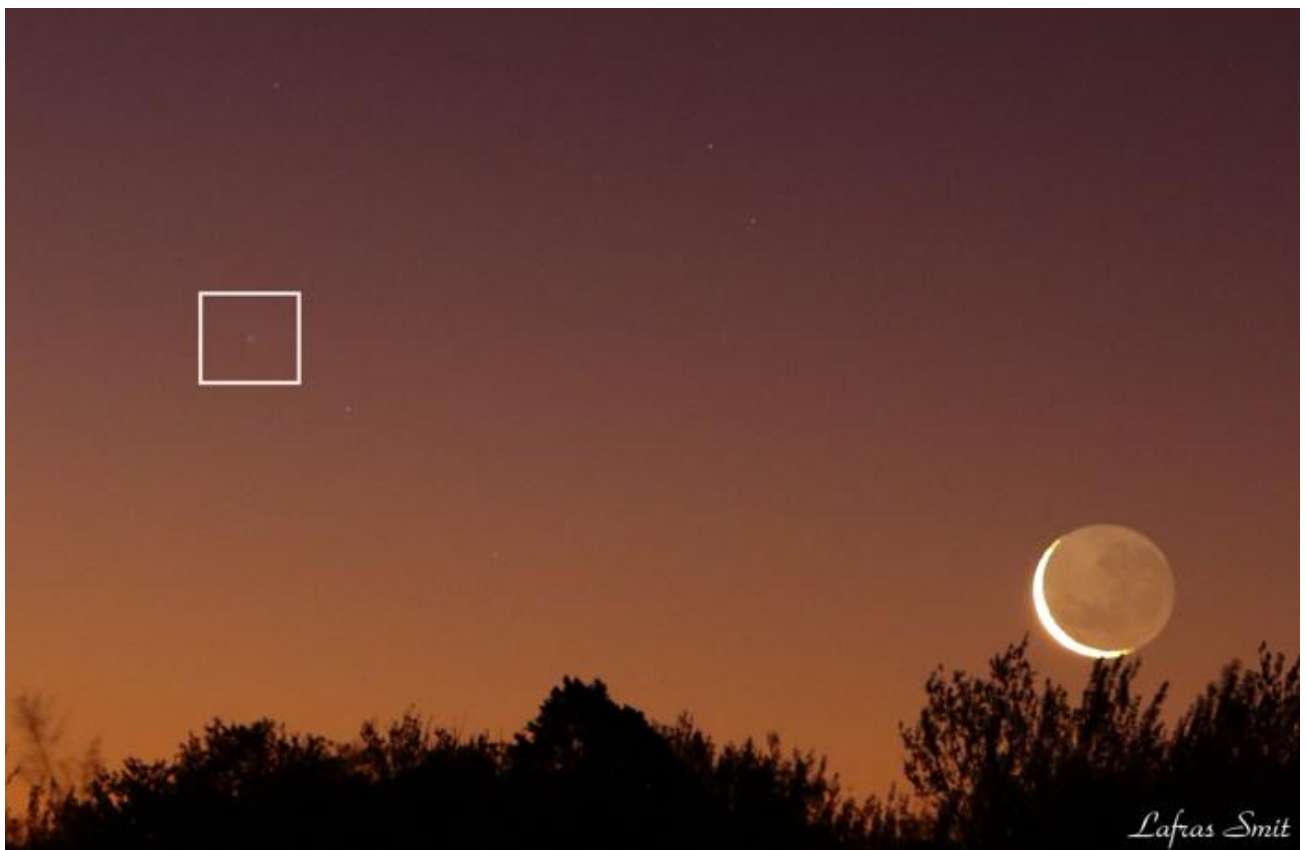


Fig 1. Image by Lafras Smit taken on 10 April 2024. The comet was barely discernible in bright twilight. The two-day old waxing crescent Moon was located just 3° to the lower right of the comet.

Tim Cooper searched with 16x50 binoculars up to 16h42 but could not locate the comet low down in bright twilight. By 13 April, the comet was just discernible immersed in bright twilight in an image by Oleg Toumilovitch (Figure 2).



Fig 2. Image by Oleg Toumilovitch taken on 13 April 2024. On this evening location was aided by Jupiter, 3° to the upper right of the comet. The two moons to the upper right of Jupiter are Io and Ganymede.

From mid-April, in addition to evening twilight, the Moon began to influence visibility, reaching its full phase on 23 April. Despite these interferences, Tim Cooper made the first visual observation of the comet at 16h36 on 19 April. Using 16x50 binoculars he estimated the magnitude as $m_1 = 4.0$, though the estimate was uncertain with the comet's altitude of only 8.5°, still some twilight and an 84% illuminated Moon. The same evening at 17h17, Johan le Roux produced the first image showing a tail, just under 1° long in p.a. 87°, with the comet just 5.4° above the horizon. On 21 April, coinciding with the date of perihelion, the comet was easily found by Tim Cooper using binoculars despite the near-full Moon.



Fig 3. Image by Kos Coronaios taken on 26 April in the absence of Moonlight shows the two tails, the blue ion tail and yellow dust tail. The bright coma shows green due to fluorescence, mainly due to diatomic carbon (C₂).

The first opportunity to observe the comet without hindrance from the Moon occurred on 26 April. An image by Kos Coronaios (Fig 3) taken before Moonrise shows an ion tail extending for over 1.5°, as well as a broad fan-shaped dust tail. The ion tail glows blue from ionized carbon monoxide (CO⁺), while the dust tail shows yellow due to reflected sunlight. On 28 April images by Kos and Johan le Roux agree that the ion tail had grown to 2.1° in p.a. 94°.

Following a week of inclement weather, Tim Cooper managed to observe the comet visually on 30 April under poor conditions, estimating $m_1 = 4.7$.

Naked eye visibility and development of the tail

As the comet gained elevation in early May, and with the Moon no longer posing any interference, the comet became easily visible in binoculars and was visible to the naked eye from dark-sky locations. The relatively high degree of condensation of the coma (DC) aided in locating the comet. Observing from a dark-sky site together with Magda Streicher on 2 May, Tim Cooper estimated the total cometary magnitude as $m_1 = 4.6$, with a well-condensed coma, DC = 7, and a narrow fan-shaped tail seen in 16x50 binoculars. On 5 May he estimated the comet slightly fainter at $m_1 = 5.0$, but still easily visible to the naked eye under a dark sky. Using binoculars, a narrow fan-shaped tail extended 0.8° in p.a. 115°, brighter towards the southern edge, which was sharper, the northern edge more diffuse. The appearance to the naked eye is well seen in an image taken on 7 May by Magda Streicher (Figure 4), and the appearance in binoculars can be seen from an image taken on 12 May by Johan le Roux (Figure 4 inset).

By now the ion tail began to show considerable differences in structure from evening to evening.



Fig 4. Image taken by Magda Streicher on 7 May 2024 is a good indication of how the comet appeared to the naked eye during evening twilight. The comet was located directly below the bright star Rigel at the time. The appearance in binoculars can be seen in the image by Johan le Roux (inset) taken five days later.



Fig 5. images by Kos Coronaios taken on 5 and 9 May show the changing appearance of the ion tail over a period of a few days.

Figure 5 shows two images taken by Kos Coronaios on the evenings of 5 and 9 May. In both images the ion tail is around 1.8° in length but clear changes in structure are visible over the period of a few days including disconnections and knots, as well as short spikes close to the coma. In an image by Johan le Roux on 8 May, the ion tail can be traced to

possibly 2.8° in length and is probably the longest measured during the apparition. At this time the dust tail was visible as a broad fan, poorly defined towards south, but sharply defined in p.a. 348° . These features also show well in Figure 6 taken by Kos on 12 May 2024. The ion tail (shown as A) extends 1.2° in p.a. 127° with a short spike (B) in p.a. 137° . The ion tail shows a probable disconnection (C) at 0.5° from the coma. The dust tail is a broad fan, curved on the southward side (D) but sharply defined in p.a. 350° (E). The dust in this direction would later manifest as a bright anti-tail as the Earth crossed the orbital plane of the comet.

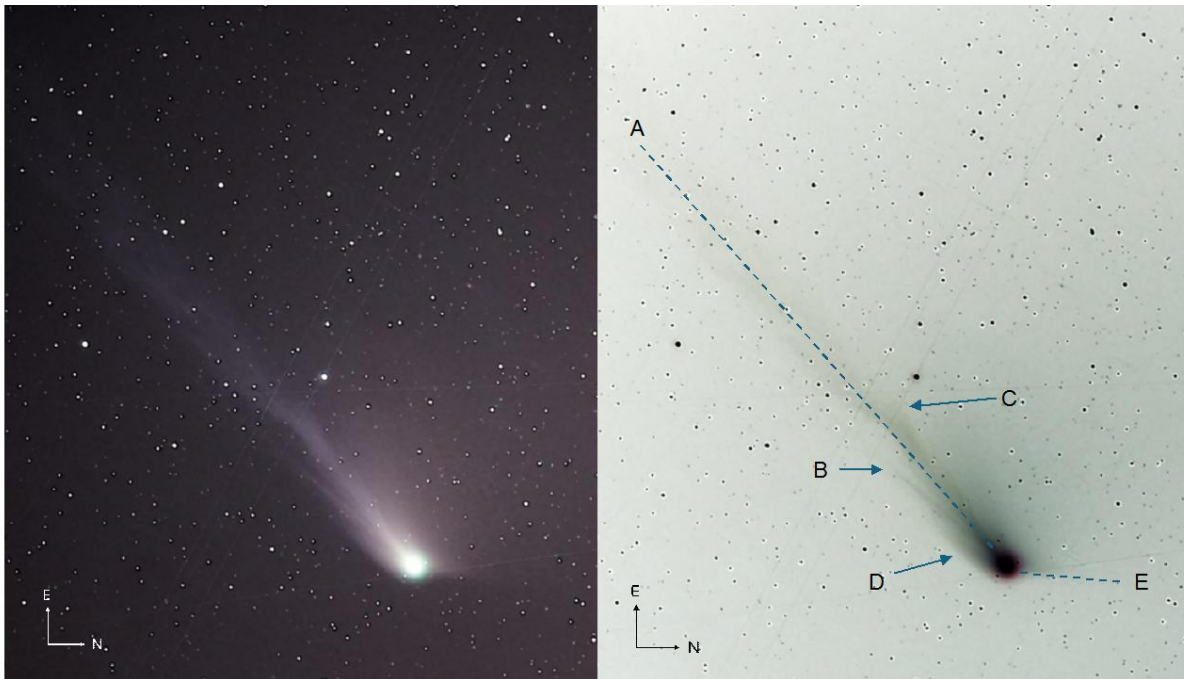


Fig 6. Image by Kos Coronaios on 12 May 2024. Several different features are visible, including a prominent ion tail with waviness or disconnection, a prominent spike, and a broad fan-shaped dust tail curved in the southern direction and spreading towards the north where it is sharply defined

Orbit crossing and the anti-tail

At times around the Earth's crossing the orbital plane of the comet, it is possible to see an anti-tail. This is not a true tail at all, but is an illusion caused by dust particles ejected into the orbit which trail the nucleus, and illuminated by sunlight are seen due to perspective in the opposite direction of the radius vector. Earth crossed this point on 6 June, and an anti-tail was predicted around this date. Images by Kos Coronaios show the sharp delineation in the dust tail in p.a. 350° became very prominent from about 18 May and is well shown in Figure 7 taken on 26 May, where the dust feature is brightest now in p.a. 344° . The closest image to time of orbit plane crossing was taken by Kos on June 7 at 18h00 (Figure 8), in which the bright anti-tail appears as a sharp

narrow spike extending 2.0° in p.a. 336° . The tail in the opposite direction extends 0.6° in p.a. 159° and is probably a combination of gas and dust tails seen in superimposition. Both tails are surrounded by diffuse nebulosity from particles above and below the orbital plane. By the time of Kos' next image on 12 June, the anti-tail was no longer visible, but the dust tail had now become the brightest feature, albeit shorter, in p.a. 330° . This dust tail became the most prominent feature as the comet faded (Figure 9).



Fig 7. Image by Kos Coronaios taken on 26 May shows the dust feature extending towards the right, in p.a. 344° , with the ion tail towards the left, in p.a. 151° . The bright star upper left is alpha Leporis, magnitude 2.6.



Fig. 8 Image by Kos Coronaios on 7 June 2024, the night after Earth crossed the orbital plane of the comet, showing the prominent anti-tail extending 2° towards the right.



Fig 9. Image by Kos Coronaios on 24 June 2024, shows the dust tail extending towards lower right as the most prominent feature.

Fading and last visibility

By end of June the comet had faded to between magnitude 8 and 9. Kos Coronaios obtained further images on 24, 27 and 30 June, as well



Fig 10. Image by Kos Coronaios on 5 July 2024. The bright star upper left is zeta Puppis (magnitude 2.2), towards lower left is the open cluster NGC 2477 and the sparse open cluster just below left of the comet is NGC 2546.

as on 5 July (Fig. 10), when the short dust tail in p.a. 304° forms the most prominent feature. The coma remains noticeably green, probably from fluorescence due to diatomic carbon (C_2) despite the distance from the Sun having increased to $r = 1.53$ AU. Kos imaged the comet on one last occasion on 29 August (Figure 11), by which time the comet had faded to magnitude 10.5, now 2.2 AU distant from the Sun, and 2.6 AU from Earth.

Chronological observations and images from Southern Africa

The complete observations and images received follow according to date. Note abbreviations used are B = binoculars; T = Schmidt-Cassegrain telescope; DC = Degree of Condensation of the coma; m1 = total cometary magnitude; p.a. = position angle of

the tail. LM = limiting magnitude, faintest star visible to naked eye. All dates are 2024 and all times are given in UT.



Fig 11. Image by Kos Coronaios on 29 August 2024. The brightest star in the trio just inside left edge is magnitude 2.6 delta Centauri. This was the last image of the comet during its 2024 return.

April 19.69, visual observation by TC, $m_1=4.0$, comet barely discernible as a faint diffuse patch in 16x50B, best seen with averted vision, possible starlike central condensation.
April 19.72, image by JIR, tail length $\sim 0.8^\circ$ in p.a. 87° .

April 20.69, visual obs. by TC, $m_1=3.9$, comet easily found in 16x50B despite twilight and bright moonlight, small round patch, quite condensed $DC=7$, with definite sharp point in the centre.

April 21.69, visual observation by TC, $m_1=4.0$, $DC=6$, coma dia. 3', possible short tail but uncertain in bright Moonlight, 16x50B.

April 26.72, image by KC (Figure 3), ion tail extends 1.6° in p.a. 99° , separates on the S side at distance 20' from the coma, where it extends in p.a. 114° . April 26.72, image by JIR, ion tail extends 1.7° in 100° .

April 28.71, image by KC, ion tail length 2.1° in p.a. 94° , dust tail curves towards N, from p.a. 117° where it is brightest, to p.a. 359° which is sharply defined. April 28.72, image by JIR, ion tail extends 2.1° in p.a. 94° .

April 29.70, image by LS, dust tail brightest in p.a. 105° , curves to p.a. 359° . Ion tail extends 1.9° in p.a. 118° . April 29.72, image by KC, ion tail curves towards S, extends 1.9° in p.a. 120° . Dust tail brightest in p.a. 111° , length 0.4° .

April 30.69, visual observation by TC, first opportunity for visual observation after a week of cloud and hazy skies, $m_1=4.7$, comet is a hazy spot with definite starlike point in the centre, no DC or coma diameter estimated as conditions poor, 16x50B. April 30.72, image by OT, tail bright in p.a. 93° , ion tail curves towards south and is 0.9° long in p.a. 114° .

May 2.70, visual observation by TC under dark skies, $LM=5.8$, $m_1=4.6$, $DC=7$, coma dia. $6'$, narrow fan-shaped tail, length 0.6° in p.a. 115° , 16x50B. May 2.71, image by KC, ion tail 1.2° in p.a. 119° , dust tail spans p.a. 124° to p.a. 5° which is straight and sharply defined.

May 3.72, image by JIR, ion tail 1.2° in p.a. 115° , dust tail is a broad curved fan, spanning p.a. 125° to 352° where it is sharply defined.

May 4.71, image by KC, ion tail extends outside field of view, $>1.3^\circ$ in p.a. 118° , dust tail spans 127° to 360° .

May 5.68, visual observation by MS, comet bright, coma dia. $6'$, much brighter towards the centre, faint star on edge of coma, $DC=6$, 40cmT x98. May 5.70, visual observation by TC, comet seems distinctly fainter, $m_1=5.0$, $DC=6$, coma dia. $5'$, tail is a narrow fan, length 0.8° in p.a. 115° , brighter towards the southern edge which is sharper, northern edge more diffuse, 16x50B. May 5.72, image by KC (Figure 5 left), ion tail 1.7° in p.a. 122° , disconnected 1.3° from the coma in p.a. 119° , shorter spike in p.a. 144° , dust tail is a broad fan diffuse towards S, but sharply defined in 348° .

May 6.70, visual observation by TC under dark skies ($LM=6.2$) comet easily visible to the naked eye and could be followed to altitude $<5^\circ$ above the horizon. In 16x50B, $m_1=5.0$.

May 7.70, visual observation by TC, comet visible to the naked eye. In 16x50B $m_1=5.2$. Tail is a narrow fan, length 0.6° in p.a. 115° . Image by MS (Figure 4) taken on a cell phone shows well the naked eye appearance of the comet.

May 8.73, image by JIR, ion tail 2.8° in p.a. 127° , dust tail is a short broad fan extending to p.a. 360° .

May 9.70, visual observation by TC from dark sky site, $LM=6.2$, comet glimpsed with the naked eye using averted vision. In 16x50B $m_1=5.3$. May 9.71, image by KC (Figure 5 right), ion tail 1.8° in p.a. 130° but considerable wavy structure, not straight, dust tail

spans from roughly p.a. 140° to 100°, then fainter to p.a. 2°. May 9.72, image by WF, overall appearance is like a shuttlecock, ion tail length 1.0° in p.a. 135°, dust tail bright to p.a. 112°, but extends fainter to p.a. 357°.

May 10.70, image by AB, tail brightest in p.a. 125° and extends for about 1°.

May 12.71, image by KC (Figure 6), ion tail 1.2° in p.a. 127°, spike 22' in p.a. 137°, ion tail shows a disconnection 0.5° from coma in 126°, gas tail is a broad fan, curved on the southward direction but sharply defined in p.a. 350°. May 12.72, image by JIR (Figure 4 inset), wide angle view, tail brightest in p.a. 128°, extends for 0.7°.

May 18.72, image by KC, ion tail extends 1.1° in p.a. 144°, dust feature in p.a. 350° becoming pronounced.

May 19.73, image by KC, similar to prev., ion tail extends 1.6° in p.a. 145°.

May 20.72, image by JIR, wide angle view shows ion tail 0.75° in p.a. 145°, dust tail extends to 334°.

May 26.71, image by KC (Figure 7) following several nights of poor weather and bright Moon, prominent dust feature visible for 0.5° in p.a. 344°; ion tail in p.a. 151°, split into two branches 26' from the coma, both branches extend equidistant to about 1° length.

June 7.75, image by KC (Figure 8), bright anti-tail appears as a sharp spike, length 2.0° in p.a. 336°, ion tail 0.6° in p.a. 159°. Both tails are surrounded by diffuse nebulosity.

Jun 12.71, image by KC, dust tail is a narrow spike 27' in p.a. 330°, ion tail 0.3° in p.a. 161°. Coma appears slightly elliptical along the axis of the tails, dia. = 12' x 10'.

June 24.75, image by KC (Figure 9), dust tail narrow spike 14' in p.a. 314°, ion tail short and not easily discerned, 10' in p.a. 166°.

June 27.68, image by KC, dust tail 15' in p.a. 315°, ion and dust tail probably indistinguishable from each other, very short extension of coma in p.a. 169°.

June 30.72, image by KC, coma dia.7', distinct green colour, tail 0.3° in p.a. 310°.

July 5.72, image by KC (Figure 10), dust tail, short, triangular appearance, 0.3° in 304°.

August 29.75 image by KC (Figure 11), tail is a narrow fan, 0.4° in p.a. 244°, last image.

Key to observers

AB = Angus Burns, Newcastle, KwaZulu Natal; JIR = Johan le Roux, Western Cape; KC = Kos Coronaios, Pearly Beach, Western Cape; LS = Lafras Smit, Kroonstad, Free State; MS = Magda Streicher, Polokwane, Limpopo; OT = Oleg Toumilovitch, Somerset West,

Western Cape; TC = Tim Cooper, Bredell, Gauteng; WF = Wim Filmalter, Riversdale, Western Cape.

Exposure details of images

Figure 1; 10 April 2024, Lafras Smit, Canon EOS 90D with Canon f/2.8 70-200mm lens at 80mm, ISO400, 3 seconds exposure at f/2.8.

Figure 2, 13 April 2024, Oleg Toumilovitch at 17h17, Canon EOS 550D with 300mm lens at f/5.6, single 0.8 second exposure at ISO1600.

Figure 3, 26 April 2024, Kos Coronaios at 17h11, Canon EOS 5D, 200mm lens at f/2.8, 15x6 second exposures at ISO6400.

Figure 4, 7 May 2024, Magda Streicher at 16h48, iPhone 15, 26mm at f/1.6, handheld for several seconds with image stabilization.

Figure 4 inset, 12 May 2024, Johan le Roux, Canon EOS 2000D, 85mm lens at f/1.8, 3.2 seconds exposure at ISO 1600.

Figure 5 left panel, 5 May 2024, Kos Coronaios, Canon EOS 5D, 200mm Canon EF lens at f2.8m, 15x30 seconds at ISO 6400.

Figure 5 right panel, 9 May 2024, Kos Coronaios, Canon EOS 5D, 200mm Canon EF lens at f2.8, 42x30 seconds at ISO 3200.

Figure 6, 12 May 2024, Kos Coronaios at 17h02, Canon EOS 5D, 200mm EF lens at f/2.8, 27x30 second exposures at ISO 3200.

Figure 7, 26 May 2024, Kos Coronaios at 17h02, Canon EOS 5D, 200mm EF lens at f/2.8, 31x30 second exposures at ISO 6400.

Figure 8, 7 June 2024, Kos Coronaios at 18h06, Canon EOS 5D, 200mm EF lens at f/2.8, 47x30 second exposures at ISO 6400.

Figure 9, 24 June 2024, Kos Coronaios at 18h06, Canon EOS 5D, 200mm EF lens at f/2.8, 45x30 second exposures at ISO 6400.

Figure 10, 5 July 2024, Kos Coronaios at 16h42, Canon EOS 5D, 200mm Canon EF lens at f2.8, 41x40 seconds at ISO 6400.

Figure 11, 29 August 2024, Kos Coronaios at 17h53, Canon EOS 5D, 200mm EF lens at f/2.8, 29x30 second exposures at ISO 8000.

Acknowledgements

Orbital elements and close approach data are from Jet Propulsion Laboratory, Small-Body Database Lookup, <https://ssd.jpl.nasa.gov/tools/>, accessed on 21 April 2024. Comet magnitudes on specific dates, other than visual observations by ASSA observers listed, are from Comet Observation Database (COBS), credit to Observatory Črni Vrh and available at cobs.si.

References

Chambó Bris, J. J., (2024), Cometografía, website of José Joaquín Chambó Bris at <https://cometografia.es/cometa-12p-pons-brooks/>, accessed on 21 April 2024.

Chandler, S.C. Jr., (1883). On the outburst in the light of the comet Pons-Brooks Sept. 21-23, *Astronomische Nachrichten*. 107 (9), pp131–133.

Green, D. W. E., (2023) Comet 12P/Pons-Brooks, Electronic Telegram No. 5280 dated 2023 July 21. Central Bureau Electronic Telegrams.

James, N., (2023), Comet 12P/Pons-Brooks outbursts continue, posted on the BAA website on 2023 November 26, https://britastro.org/section_news_item/comet-12p-pons-brooks-outburst-continue.

James, N., (2024), 12P/Pons-Brooks small outburst 2024 Feb 29. See also light curves posted on the BAA website 2024 March 1, https://britastro.org/section_news_item/12p-pons-brooks-latest-lightcurve.

Kronk, G. W., (2008). 12P/Pons-Brooks, at Cometography.com. Archived from the original on 5 July 2008. Retrieved 7 May 2009.

Kronk, G. W., (2024), details from Cometography website of Gary Kronk at <https://cometography.com/pcomets/012p.html#>, accessed on 21 April 2024.

Tomko, D. and Neslušan, L., (2016), Meteoroid stream of 12P/Pons-Brooks, December κ -Draconids, and Northern June Aquilids, *A&A* 592, Article number 107, <https://doi.org/10.1051/0004-6361/201628404>

Yoshida, S., (2024), <http://www.aerith.net/comet/catalog/0012P/2024.html>, accessed on 15 December 2024

The **Astronomical Society of Southern Africa** (ASSA) was formed in 1922 by the amalgamation of the Cape Astronomical Association (founded 1912) and the Johannesburg Astronomical Association (founded 1918). It is a body consisting of both amateur and professional astronomers.

Publications: The Society publishes its electronic journal, the *Monthly Notes of the Astronomical Society of Southern Africa (MNASSA)* bi-monthly, the annual *Sky Guide Southern Africa*.

Membership: Membership of the Society is open to all. Please consult the Society's web page : <https://assa.saao.ac.za> for details. Joining is possible via a local Centre or as a Country Member.

Local Centres: Local Centres of the Society exist at Bloemfontein, Cape Town, Durban, Hermanus, Johannesburg, Pretoria and the Garden Route Centre; membership of any of these Centres automatically confers membership of the Society.

ASSA Council	
President	Derek Duckitt
Vice-President (outgoing)	Dr Daniel Cunnama
Vice President (Incoming)	Prof Matie Hoffman
Membership Secretary	Andre Bruton
Treasurer	Adv AJ Nel
Secretary	Lerika Cross
Council Member	Case Rijdsdijk
Council Member	Dr Ian Glass
Bloemfontein Chair	Prof Matie Hoffman
Cape Chair	Willem Brazelle
Durban Chair	Mike Hadlow
Garden Route Chair	Peter Hers
Hermanus Chair	Derek Duckitt
Johannesburg Chair	John Lindsay-Smith
Pretoria Chair	Johan Smit
Council Appointees	
Scholarship Convenor	Dr Claire Flanagan
ASSA Communication Coordinator	Martin Heigan
Webmaster	John Gill
Section Directors	
Dark Sky	Dr Daniel Cunnama
Observing (dark and shallow sky)	Colin Steyn
Photometry, Spectroscopy	David Blane (caretaker role)
Cosmology, Astrophysics	Derek Duckitt
Archives/History	Chris de Coning
Double and Variable Stars	Dave Blane
Astrophotography	Martin Heigan
Instrumentation and ATM	Chris Stewart
Comet, Asteroid and Meteor (CAM)	Tim Cooper
Outreach	Dr Pierre de Villiers
Solar	Jacques van Delft
Planetary	Clyde Foster

mnassa

monthly notes of the astronomical society of southern africa

Volume 84 Nos 1-2

February 2025

Table of Contents

News Note: Dr Rosalind Skelton appointed Managing Director of the SAAO	1
News Note: International Microlensing Conference and Official Opening of PRIME Telescope	3
At last, a whisper of SN 1987A!	4
Re-imagining the Planetarium as the Wits Anglo American Digital Dome	9
Unravelling the Sun: A Year of Solar Activity in 2024.....	18
Observations and images of Comet 12P/Pons-Brooks.....	41